Politecnico di Torino

MSc in Energy and Nuclear Engineering

–

Sustainable Nuclear Energy

Effects of solid moderators on the neutronic performance of a SNR

Supervisors:

Dr. Nicolò Abrate

Prof. Sandra Dulla

Dr. Roberto Pergreffi

Candidate:

Edoardo Traverso

Abstract

This work aims at evaluating the effects of solid moderators on the neutronic performance of the space nuclear reactor of 500 kW_{th} space nuclear reactor currently being developed within the SELENE project to supply energy to a lunar base. The thesis supports the core design activities carried out by ENEA within the SELENE project, which aims to develop a reactor core for lunar applications. To this end, five solid moderators were examined: beryllium (Be), beryllium oxide (BeO), graphite, zirconium hydride ($ZrH_{1.6}$) and yttrium hydride ($YH_{1.85}$). The comparison was carried out in terms of key neutronic parameters, including the multiplication factor, moderation ratio curve, neutron spectrum, axial power distribution, and reactivity swing over a 10-year lifetime. All calculations were performed using the Serpent Monte Carlo code on a preliminary model of the SELENE reactor fuel assembly, in order to better assess the physical behavior of the different configurations. The results indicate that the two metal hydrides represent the most promising solutions, offering an optimal compromise among the investigated parameters. In particular, $ZrH_{1.6}$ emerges as the most suitable moderator for the SELENE concept, as it combines the highest initial multiplication factor with the lowest reactivity swing. $YH_{1.85}$, although slightly less effective, represents a valid alternative. However, it should be noted that this conclusion relies on the assumption of constant density in the metal hydrides, i.e., neglecting variations in hydrogen content due to temperature and concentration gradients. Maintaining this condition would likely require the implementation of an ad hoc barrier, which is out of the scope of this work.

Contents

List of Figures

List of Tables

List of acronyms

ASI	Agenzia Spaziale Italiana
BC	Boundary Condition
BOL	Beginning Of Life
CM	Center of Mass
EOL	End Of Life
FA	Fuel Assembly
FC	Fuel Compact
HALEU	High Assay Low Enriched Uranium
HEU	Highly Enriched Uranium
HP	Heat Pipe
HRS	Heat Removal System
HTGR	High Temperature Gas-cooled Reactors
ILRS	International Lunar Research Station
LOCA	Loss Of Coolant Accident
MEnH	Moon Energy Hub
MR	Moderating Ratio
NASA	National Aeronautics and Space Administration
PWR	Pressurized Water Reactor
RTG	Radioisotope Thermoelectric Generator
SELENE	Sistema Energetico Lunare con L'Energia NuclearE
SDP	Slowing-Down Power

SI	Spectral Indexes
SLS	Space Launcher System
SNR	Surface Nuclear Reactor
TRISO	TRi-Structural ISOtropic particle fuel
TRL	Technology Readiness Level

1 Introduction

The renewed interest in establishing a prolonged human presence beyond low Earth orbit has brought the Moon back to the centre of international space strategies, both as a scientific laboratory and as a natural outpost for future missions to other bodies of the Solar System, notably Mars. In this context, the Moon is increasingly seen not only as an object of mystery and exploration, but as the first step towards an interplanetary human civilisation, with very advanced concepts such as lunar villages. Several major nations have now exposed their lunar missions roadmaps that show a strong incline to long term missions: NASA's Artemis programme foresees a return of humans to the lunar surface, with a particular focus on the south polar region, taking the Moon as a permanent infrastructural element in a broader exploration framework; the China–Russia International Lunar Research Station (ILRS) project similarly aims at a permanent robotic and eventually human crew infrastructure on the Moon, targeting full deployment before 2035 and explicitly positioning the outpost as a hub for subsequent deep-space missions. Among the vast and numerous technological challenges associated with any kind of space mission, having a reliable and continuous electrical power supply is universally recognized as one of the main requirements for any long-term lunar base. Electrical power is needed not only to power life-support systems, thermal control, communications and surface mobility, but also to operate scientific research activities and, more generally, any kind of asset that justifies the need for a human outpost on the Moon. Several options are available to supply electrical power in space, each with specific advantages and limitations based on the respective peculiarities. Photovoltaic systems are an attractive solution whenever sunlight is available, since they rely on a technology with no moving parts and high technology readiness. However, the order of magnitude of the energy needed for this specific task quickly discards this option due to the really low ratio of kWh produced per surface of panel, even ignoring the fact that a lunar day lasts 14 of earth ones; furthermore, a dusty atmosphere like the lunar one would degrade their performance over a relatively short amount of time. Radioisotope Thermoelectric Generators (RTGs) have a long and successful history in deep-space satellites and planetary rovers, exploiting the heat of alpha-emitting radioisotopes (typically Pu-238) converted to electricity via thermocouples. They offer exceptional reliability, no moving parts and mission lifetimes of several decades, making them ideal for low-power applications in very remote or harsh envi-

ronments. Nevertheless, as said, their specific power is very low and their efficiency modest, so, scaling RTGs to an adequate power level for a full human outpost would require prohibitive amounts of radioisotope fuel and system mass, making them unsuitable as the primary power source for this application. Nuclear fission reactors represent another option, building on decades of experience with terrestrial reactors as well as on a series of specific space reactor concepts. These systems can provide continuous power over many years, are largely independent of the external environment and can achieve very high power densities, resulting in compact and relatively lightweight plants capable of operating in the extreme thermal, vacuum and radiation conditions of the lunar surface. The comparison of these technologies against the requirements of future lunar bases highlights a simple but important fact: there is no intrinsically perfect electricity source to choose from; every space mission has its own foreseen duration, payload limitation and a specific objective. It is possible, anyway, to classify each technology on the basis of its power output and the time span of utilization, like IAEA did in Figure 1

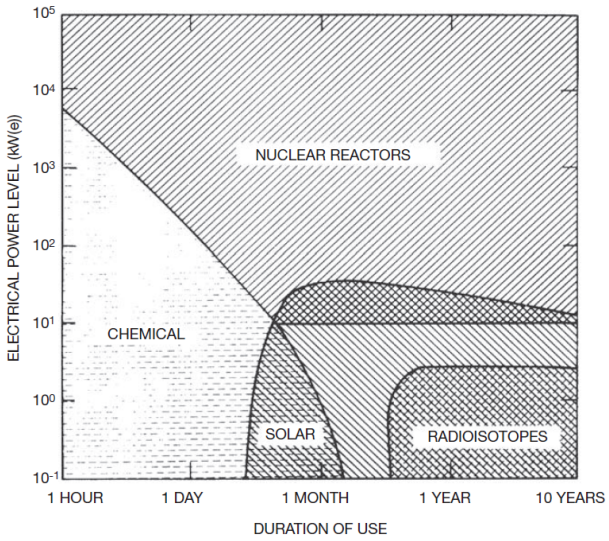

Figure 1: Classification of power sources in space, IAEA (2005)

As it can be seen, nuclear fission reactors are widely regarded as the only viable option to supply robust, resilient and continuously available high power levels to lunar activities; radioisotopes find their main applications, for example, on deep space satellites which require minimal electricity load for a very long time span; while solar technologies, as said previously, are unable to achieve high electrical power levels due to their intrinsic structural and meteorological limitations.

1.1 SELENE project

This technological landscape has prompted several national space agencies to initiate dedicated programmes on surface nuclear power for the Moon. The Italian Space Agency (ASI) has decided to develop its own contribution to a lunar base and, with this objective, launched a call for proposals to finance three complementary projects: two focusing on the planning of the Moon experimental campaign and the third on the design of an adequate power source. Among the winners were the SELENE (Sistema Energetico Lunare con L'Energia NuclearE) project, part of the concept of a Moon Energy Hub (MEnH), an infrastructure responsible for the production, storage and distribution of thermal and electrical energy based on one or more surface nuclear reactors. This collaboration between ENEA, Thales Alenia Space and Department of Energy of the Politecnico di Milano has the main objective of advancing the design maturity and Technology Readiness Level (TRL) of the MEnH, paving the way for its future industrialisation and deployment. This requires the development of innovative technological solutions for managing a Surface Nuclear Reactor (SNR)-based energy infrastructure tailored for every planned activity, while meeting stringent criteria of operability, reliability and compactness in the lunar environment.

For what concerns the reactor core design, SELENE aims to identify a suitable geometric and material configuration capable of delivering the required power over the mission lifetime, while respecting the size and mass constraints imposed by available launchers and landers; the target electrical power is set to be 100 kW_e (500kW_{th}) over an estimated period of 10 years, with a total system mass below 8 tonnes. Based on a previous feasibility study in which several options are compared [3], some design choices were adopted regarding the fuel, namely TRi-Structural ISOtropic particle fuel (TRISO) particles with uranium-235 enrichment below 20 wt%, the heat removal system, which uses heat pipe technology and the moderator, which is required to be a solid material. On this latter concept, which is very peculiar, the rationale is that liquid moderators, even if representing the industry standard in 'terrestrial' technologies, present some challenges that very quickly rules them out from space application: on one hand, fluids in lunar microgravity would present very complex dynamics that would need dedicated control systems, on the other hand, by choosing solid moderators, every additional active hydraulic and pressurization system would not be needed drastically lightening the design.

1.2 Aim of the work

This work evaluates the different solid moderators' effect on the neutronic performance of the SELENE SNR. Five materials acting as solid moderators have been chosen: Beryllium (Be), Beryllium Oxide (BeO), Graphite (Gr), Zirconium hydride (ZrH_X) and Yttrium hydride (YH_X). After having contextualized the theoretical background of neutron transport and moderation, the SELENE reactor design and the methodology chosen for the evaluation of those moderators, the results, obtained with the Monte Carlo code Serpent, will compare different features and parameters regarding the overall neutronic performance of the reactor. In the end, a comprehensive overview, based on the overall findings, will allow to elect which solid moderator fits better in this framework.

2 Theoretical background

This chapter introduces the pivotal role of neutron moderation in impacting the behaviour of thermal reactors and sets the theoretical background of what will come next: assessing the impact of different solid moderators on the neutronic performance of the SELENE reactor. To justify the presence of a moderator in the first place, it is necessary to reiterate that the technology from which this project takes place, is a thermal spectrum reactor coupled with common fissile fuels, specifically HALEU. This quickly brings up one of the main aspects that rules fission physics inside of a nuclear reactor: the fission cross section of the fissile U-235, function of incident neutron energy and shown in Figure 2.

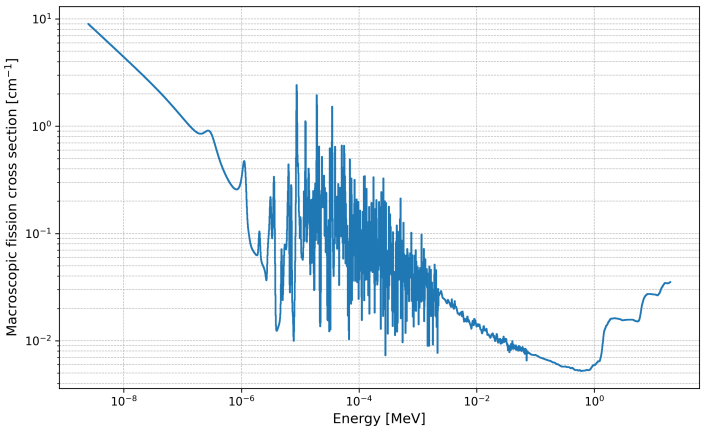

Figure 2: Macroscopic cross section of U-235

In a typical fission event, prompt neutrons are born 'on the right' of this spectrum, with energies of around 2 MeV. Still, as can be seen in Figure 2, the cross section peak (highest probability of inducing fission) is found on the opposite side of the distribution, so neutrons need to undergo a sequence of scattering events in the surrounding medium in order to lose energy and move across the spectrum towards the thermal region, where fission probability is maximized; at this point, according to many factors, like the nature of the medium, part of the neutrons will eventually reach thermal equilibrium with the moderator ($E \approx kT$). This process is conventionally divided into a slowing-down domain and a thermalisation domain and, again, is heavily dependent on the surrounding materials; the moderator in particular can be defined, in first approximation, as a

central component that has to maximize the slowing-down and thermalization of neutrons while, at the same time, minimizing its absorption. To better understand this phenomenon and interpret the results shown in this work, it is crucial to expand on the main mechanisms that rule neutron motion, the characterization of a moderator from the physical point of view and the different ways of defining their effectiveness.

2.1 Neutron slowing down

The so called neutron slowing down is the set of processes by which fast neutrons, emitted by fission, lose kinetic energy through collisions with the surrounding media until they reach the epithermal and then eventually the thermal range, where, as shown above, most of the fissile isotopes have much larger fission cross sections. In a thermal reactor, like in this case study, slowing down is not only about reaching the optimal energy/speed maximizing fissions but also about surviving while crossing the resonance region (characterized by the spiky region in Figure 2), where capture resonances can remove neutrons and therefore strongly affect the feasibility and performance of the system. For this reason, the slowing-down theory is usually introduced as part of a broader spectrum description: a fission source at high energy, a slowing-down/epithermal domain, and eventually a thermalization domain at low energy. In the slowing-down domain, it is assumed that the vibrational motion of the nuclei around their equilibrium positions in the crystal lattice is negligible and that the effect of chemical or lattice binding on the scattering process is also negligible, so that the target nuclei can be regarded as free and effectively at rest before the collision.

By taking into account those hypothesis, starting the description of the energy cascade on the fast side of the spectrum, it can be said that in the slowing-down domain, elastic scattering is the dominant energy-loss mechanism and can be treated as a classic two-body collision between a neutron and a target nucleus, which under the above assumptions is considered as a free nucleus initially at rest. The standard derivation utilized in this context is the conservation of momentum and kinetic energy in the centre of mass (CM) reference frame, where an elastic collision corresponds to a change in direction of the neutron velocity while keeping its magnitude unchanged; switching to the laboratory frame gives the unknown final neutron kinetic energy as a function of A, the ratio of the mass of the target nucleus to the mass of the neutron, and of the CM scattering angle, $\cos(\theta)$ [19].

$$\frac{E_{n,f}}{E_{n,i}} = \frac{A^2 + 1 + 2A\cos(\theta)}{(A+1)^2} = \frac{1}{2}[1 + \alpha + (1-\alpha)cos(\theta)] \tag{1}$$

A very important parameter emerging from this calculations is the α factor, which includes in itself lots of physical significance: it is defined as the minimum ratio between the final energy and the initial energy of a neutron after a collision, or in other words a magnitude estimation of the energy loss per scattering event in function of a certain target nucleus defined in A

$$\alpha = \frac{(A-1)^2}{(A+1)^2} \tag{2}$$

This already gives insight into the reason for which light nuclei are effective moderators: smaller A leads to smaller α and therefore identifies a possibly larger single-collision energy loss, while large A implies α close to 1 and therefore small fractional losses per collision. To further characterize the practical treatment of moderation, one also should specify an angular scattering law; a widely used idealization (still is an approximation) in this region, is isotropic scattering in the CM frame, which means that the neutron is equally likely to emerge in any CM direction: the cosine of the scattering angle, $\mu = \cos(\theta)$, is uniformly distributed over $[-1, 1]$. It is fundamental to see also that the outgoing energy ratio $E_{n,f}/E_{n,i}$, defined in equation 1 is bounded between the two kinematic limits [α,1]; due to the fact that μ is uniform and the outgoing energy ratio $E_{n,f}/E_{n,i}$ depends linearly on μ, it follows that the post-collision neutron energy is uniformly distributed in $[\alpha E, E]$ [19]. This result is particularly valuable for slowing-down theory because it provides a simple, closed-form probability law linking the "angle randomness" of scattering to a tractable energy-loss distribution.

At this stage, it becomes important to leave energy E as a unit measure, since moderation is fundamentally a multiplicative energy cascade and the law of elastic collision is defined with the said energy ratio, the concept of lethargy u, introduced by Fermi, needs to be shown:

$$u = \ln \frac{E_{ref}}{E} \tag{3}$$

u is the natural logarithm of neutron kinetic energy, which increases as neutrons slow down; the reference energy is arbitrarily chosen to normalize and to keep the argument dimensionless. As said, the key advantage is that the cumulative slowing down becomes additive and independent from the absolute energy scale: each collision produces a lethargy gain $w = \Delta u$ that can be written like this:

$$u_f - u_i = \Delta u = -\ln \frac{A^2 + 1 + 2A\cos(\theta)}{(A+1)^2} \tag{4}$$

so that the slowing from E_f to E_i corresponds to a single lethargy interval $\Delta u = ln\frac{E_{nf}}{E_{n,i}}$. Another very important parameter, which is closely linked to the latter, is the average logarithmic energy decrement ξ: it is defined as the mean lethargy gain per elastic collision, i.e. the expected value of lethargy gain u under the adopted scattering law. The main utility of deriving this value is that ξ is a function of A only (under the isotropic-CM elastic model), so it provides a simple way of comparing moderators at the level of single-collision efficiency

$$\overline{\Delta u} = \xi = 1 - \frac{(A-1)^2}{2A} ln(\frac{A+1}{A-1}) \tag{5}$$

Once ξ is known, also the mean number of collisions required to slow a neutron from E_i to E_f is simply obtained by dividing the intended lethargy change by ξ:

$$n = \frac{u}{\xi} \tag{6}$$

It is important anyway, to remember that all these parameters are extremely useful for contextualizing reactor moderation, but they carry their stochastic nature being dependant on the chosen scattering law.

The final step of this discussion has to be the slowing-down equation, which turns the parameters and single-collision physics discussed until now into a complete spectrum balance for the whole neutron population; the logic resembles the one of transport equation but is specifically written to describe moderation in the slowing-down region, where the dominant process is scattering from higher to lower energies. With the assumption of an infinite homogeneous medium, to simplify the physics description, the equation can be written as a balance that equates: on the left, the rate at which neutrons scatter into a certain lethargy interval from a higher point by summing the source term $S(u)$ and the arrival density $\rho(u)$; on the right, the reaction rate of 'exiting' out of that lethargy interval through absorption.

$$S(u) + \rho(u) = \Sigma(u)\phi(u) \tag{7}$$

By expanding the arrival density and writing the integral for the interval $[u-\epsilon, u]$, where ϵ is the maximum lethargy gain per scattering event, the classic form of the slowing down equation for the flux is found [19]:

$$S(u) + \int_{u-\epsilon}^{u} \Sigma_s(u')\Phi(u')P(u-u')du' = \Sigma(u)\phi(u) \tag{8}$$

where:

- $S(u)$: source term of neutrons entering lethargy interval $[u + du]$
- $\Sigma_s(u')\Phi(u')P(u-u')$: scattering rate to lethargy interval $[u + du]$ multiplied by transfer probability
- $\Sigma(u)\phi(u)$: removal rate from lethargy interval $[u + du]$

In this form of the slowing-down equation, the unknown is the lethargy dependent neutron flux, while the given quantities are the external source, the macroscopic cross sections and the transfer probabilities kernel which is determined by the elastic-scattering model discussed at the beginning of the chapter. The main difficulty is that the equation has no closed-form solution except in special simplified situations; so the way around is to utilize numerical solvers: starting from discretization of lethargy into groups, then approximate the integral by group-to-group transfer probabilities (P_{kernel}), and solving the resulting linear system from high to low energy.

2.2 Characteristic parameters of a moderator

In the previous chapter, the moderation process was analysed in terms of individual collisions (elastic scattering laws), lethargy and average logarithmic energy decrement ξ and the slowing-down equation written in lethargy space. On that basis, a real moderator can be characterised by a small set of macroscopic parameters which condense the microscopic scattering and absorption cross sections into figures of merit directly usable in reactor design: the slowing down power (SDP), the moderating ratio (MR), and the slowing down length. These parameters connect the kinetic description of slowing down with integral reactor quantities such as resonance escape probability, thermal utilisation factor, and migration length which, will be analyzed in the next paragraph where neutron thermalization will be discussed.

2.2.1 Slowing Down Power (SDP)

For a monatomic moderator with atomic mass A, the average logarithmic energy decrement per collision was derived in equation 5 and is defined as the mean increase of lethargy per elastic collision. The concept of SDP is strongly bounded to this one and can be seen through its definition below; under the assumptions of elastic, isotropic scattering in the CM system, the slowing down power is then:

$$SDP = \xi \ \Sigma_s, \tag{9}$$

with:

- ξ, average logarithmic energy decrement
- Σ_s, scattering cross section.

This quantity has the dimensions of an inverse length and can be interpreted as the average lethargy gain per unit path length; in other words, SDP gives more insight into moderator performance, incorporating other than the pure kinematics effect (quantified in ξ), also the interaction probability through Σ_s. Light nuclei (small A) have large ξ and, when combined with a sufficiently large Σ_s, yield a high SDP, which is one of the reasons why hydrogen is widely considered a very effective moderator.

2.2.2 Moderating Ratio (MR)

While the SDP of a certain moderator measures how fast neutrons are slowed down, it does not account for the competitive mechanism of absorption during the slowing-down process. A good moderator must not only reduce neutron energy efficiently, but also avoid capturing too many neutrons before they reach the thermal range where they can cause fission in the fuel. In reactor engineering, it is customary to define the MR as:

$$MR = \frac{\xi \ \Sigma_s}{\Sigma_a} = \frac{SDP}{\Sigma_a} \tag{10}$$

where Σ_a is the macroscopic absorption cross section of the material in the thermal range (or an appropriately averaged absorption over the energy interval of interest). A large moderating ratio indicates a material that combines efficient slowing down (large $\xi \ \Sigma_s$) with weak absorption (small Σ_a), which is precisely what is desired for an "almost transparent" moderator. Heavy water and graphite owe their widespread use in natural-uranium reactors to their very high moderating ratios, which allow a sufficient

fraction of neutrons to survive slowing down and reach the low-energy domain where they can be absorbed in fertile and fissile nuclides.

2.3 Neutron thermalization

In the slowing down range, neutrons lose energy mainly by elastic scattering on nuclei that are treated as free and at rest in the laboratory frame. Under these assumptions collisions always decrease the neutron energy: after each collision, the outgoing energy E' is bounded above by the incoming energy E, and the average logarithmic energy decrement per collision ξ is positive.

In the thermal energy domain instead, neutron interactions with matter can no longer be treated using the simplifying assumptions valid for the slowing-down range: the key physical distinction arises because neutron energies become comparable to the characteristic ones of lattice vibrations and molecular rotation/translation (E $\approx$ kT $\approx$ 0.025 eV at room temperature), so target nuclei cannot be regarded as free and at rest: they undergo thermal agitation and are bound in a solid or liquid, requiring a description that accounts for the thermal motion of the moderator atoms. The critical consequence is that neutrons no longer slow down monotonically through elastic scattering off nuclei at rest, but thermalisation involves a two-way energy exchange: neutrons can gain or lose energy depending on whether they collide head-on with a faster-moving nucleus or 'overtake' a slower one. A fundamental aspect to discuss is how to treat the transition between slowing down and thermal region, since it drastically changes the moderation physics; in numerical modelling, an arbitrary cut-off energy (E_{cutoff}) has to be chosen and in general, corresponds to the equilibrium between neutrons and matter; the methodology of how thermal scattering is treated in the Monte Carlo Serpent code, is going to be discussed in depth in the dedicated Chapter 6.

Proceeding in a similar manner to the paragraph dedicated to the slowing down region, thus introducing the main concepts leading to understanding the characteristic equation, it is necessary now to present what the neutron spectrum looks like in the thermal region. At equilibrium, and in the hypothetic absence of absorption, it would be a so called Maxwell spectrum; it has been well observed in materials with low capture when in sufficient enough volume, the expression is the following:

$$n(E)dE = \frac{2\sqrt{\frac{E}{kT}}}{\sqrt{\pi}} e^{-\frac{E}{kT}} \frac{dE}{kT} \tag{11}$$

Before introducing the thermalization equation, there are two other points to make to

contextualize the phenomena:

- **Principle of microreversibility**: stressing again the hypothesis of absence of absorption and equilibrium, when the neutron spectrum is the Maxwell spectrum, there are exactly the same number of transfers by diffusion from an energy interval dE to an energy interval dE' as transfers in the opposite direction, from dE' to dE. This leads to a mathematical constraint on the transfer relationship $P(E' \rightarrow E)$ that any model would have to observe:

$$E\ e^{-\frac{E}{kT}}\ dE\Sigma_s(E)\ P(E \rightarrow E')\ dE' = E'\ e^{-\frac{E'}{kT}}\ dE'\Sigma_s(E)\ P(E' \rightarrow E)\ dE \quad (12)$$

  product between the Maxwellian flux, scattering cross section and transfer probability.

- **Scattering equations**: the double differential (by energy and by angle) thermal scattering cross section, $\Sigma(E')P(E' \rightarrow E)P(\mu)$, is a function of three variables E', E and μ which can in fact be expressed by S, a function of only two variables, $S(\alpha, \beta)$.

After having clarified the most important concepts, the thermalization equation is then presented: it is derived by establishing neutron balance within the thermal domain in the interval $[0, E_{cutoff}]$, remembering that the energy boundary is the one selected to separate the epithermal with thermal range. Below is the space and time independent formulation [19]:

$$\int_0^{E_{cutoff}} \Sigma_s(E')\Phi(E')dE'P(E' \rightarrow E)\ + S_{sl-d}(E) = \Sigma_t(E)\Phi(E) \quad (13)$$

with:

- $\int_0^{E_{cutoff}} \Sigma_s(E')\Phi(E')dE'P(E' \rightarrow E)$: neutrons scattered into energy E from E' in thermal domain $[0, E_{cutoff}]$
- $S_{sl-d}(E)$: source term of neutrons that cross the cutoff and arrive in energy E from the slowing down region
- $\Sigma_t(E)\Phi(E)$: removal rate from thermal domain $[0, E_{cutoff}]$

This similarity between the slowing down equation reflects the same physical process of energy jumps by scattering but hides a completely different aspect that was

highlighted at the beginning of this paragraph: whilst in the slowing down problem we always had the outgoing energy less than, or equal, to the incoming (or lethargies u, u'), in the thermalisation problem, transfers can occur in both directions (the integral applies to the entire thermal domain).

3 The principal design considerations for the SNR in the SELENE project

The SELENE project has a big picture target of contributing to develop a MEnH, where one or more SNRs, provide continuous electrical and thermal power to a lunar human outpost. The reactor core design presents very ambitious challenges since it must reconcile stringent mass and volume constraints imposed by launch vehicle capabilities with the need for long life, highly reliable operation in the harsh lunar environment. In addition, the reactor technology choices must be adapted to a completely different scenario compared with terrestrial one. In this chapter, a contextualization of the main requirements to take into account will be made, as well as the decisions taken in terms of the main components conception, to finally conclude with an assessment of the preliminary fuel assembly (FA) design on which all the analysis of this thesis will be portrayed.

3.1 Main requirements

The system architecture is driven by a large number of different requirements that need to be tailored for a lunar base power system. Focusing on the 'nuclear' aspects, the high-level constraints defining the design boundaries are the following:

- **Compactness**: the SNR must be pre-assembled and deployed via a single launch, fitting within the payload specifications of advanced NASA's Space Launcher System (SLS). This clearly imposes strict limits on mass and volume.
- **Safety**: the structure has to withstand launch loads, landing and the hostile lunar environment characterized by low gravity, radiation, fine dust and micro meteoroid impacts. From a radiological point of view, the reactor shielding must ensure that the crew is exposed to maximum 50 mSv per year, limit that comes from the 20% of the estimated environmental lunar dose. Furthermore, the system must maintain a subcritical configuration during launch, landing, and deployment.
- **Operation and reliability**: the reactor, rated at $\approx$ 500kW$_{th}$, is required to deliver a continuous rated electrical power output of 100 kWe in the full time frame of 10 years without refuelling and significant maintenance or human intervention.

So, the design has to account for options for remote control and commissioning while assuring extreme reliability, targeting the lowest possible failure rates for safety-critical components.

- **Fuel enrichment**:historically, space reactors favored Highly Enriched Uranium (HEU) due to its high fissile density, which rightfully would allow for both extremely compact and light cores. However, new and strict international non-proliferation policies heavily restricted the production and utilization of HEU; therefore, the SELENE project turned to the use of HALEU, with a rated U-235 enrichment that must not exceed the threshold of 19.75%.

3.2 Design choices in terms of fuel, heat removal system and moderator

Based on all the above-mentioned requirements, as well as on the insights from a previous feasibility study in which several options were compared [3], the main choices for the nuclear reactor design are the following:

- **Fuel**: as a central component in the design that would shift the whole reactor structure, TRISO particle fuel has been chosen because of its excellent safety margins, high-temperature operability, manufacturing flexibility and long life. TRISO is characterized by multi-layered microspheres that enclose a kernel of fissile Uranium (potentially UN, UC, UCO, UO2) with a series of ceramic materials which exceptionally retain radioactive fission products. These particles will be embedded in a Silicon Carbide (SiC) composite matrix, which provides excellent structural integrity and acceptable neutronic transparency.

- **Heat Removal System (HRS)**: to extract thermal energy from the core, the design follows the reliability requirement by avoiding circulating fluid systems in favor of a passive approach using Heat Pipes (HPs). HPs operates passively via evaporation and condensation of a liquid metal working fluid driven by capillary action; this eliminates at the same time two critical characteristics such as any moving parts (pumps) and pressurized structures, inherently bypassing the risk of a Loss Of Coolant Accident (LOCA) and making the system suited for the lunar environment. The baseline configuration utilizes Sodium (Na) as working fluid since it behaves well in the range of temperature between 800-1200K, which is coherent with the need of targeting $\approx$ 1200K to have a high efficiency HRS.

The heat pipes also provide redundancy since the failure of a single pipe can be mitigated by the parallel ones.

- **Solid moderator**: the first consideration to make is that the choice of a thermal spectrum reactor was necessary in terms of fuel requirement, since the imposed enrichment threshold (<19.75%wt of U-235) could not have been easily guaranteed for a fast reactor. Thus, the implementation of a certain kind of moderator was obliged, but a fundamental aspect is the specification of a solid one: lunar microgravity makes fluids' behaviour very difficult to manage, furthermore, the active hydraulic and pressurization systems that would come into place would render the reactor heavier and even more difficult to deploy. The shortlist of solid moderators to analyse comprises: Beryllium (Be), Beryllium Oxide (BeO), Graphite (Gr), Zirconium hydride (Zr_x) and Yttrium hydride (YH_x).

- **Inverted FA concept**: a very specific design feature is the FA geometry, since the typical material allocations will be reversed: the classic pin-shape of nuclear fuel will be taken by the moderator, whose pins will be immersed in a fuel compact of TRISO particles immersed also in a SiC matrix. This configuration was chosen mainly for two factors: better heat extraction performances through heat pipes positioned into the fuel compact and the possibility of accomodating a larger amount of fuel between the hexagon boundary and the moderator pins.

3.3 Geometrical and material data of the preliminary fuel assembly configuration

The version of the SELENE core used in this work is shown below. It is important to underline that this version is not only preliminary but also incomplete: in fact, neither the reflector nor the control and shutdown systems are included. At the same time, it serves as a valid and consistent starting point, aligned with the design choices introduced above, for performing analyses that will inform subsequent design stages. This preliminary configuration, shown in Figure 3a, features 55 hexagonal fuel assemblies with an active length of several tens of centimeters, so as to meet the power and operability requirements necessary to deliver 100 kWe for 10 years.

At FA level, shown in Figure 3b, the standard geometry is defined by the following specifications: the inner region of the FA surrounding the five moderator rods (blue) and the two heat pipes (green) is filled by the SiC-TRISO fuel compact (FC) with a packing fraction of 0.4, here defined as the ratio in the fuel region of particles volume

and FC volume. due to fabrication reasons, all contact surfaces between the pins and the FC, as well as the axial and radial boundaries of each FA are separated by a 0.5 cm-thick layer of SiC, referred to as 'unfueled region' and therefore not part of the fuel compact.

For what concerns the chemical compositions of those materials, in Appendix A, in Table 14, are found the specifics for the TRISO particles, while in Tables 15, 16 and 17, are reported the atomic data of each HP component; moderator compositions are left for the next chapter, where each material will be presented in detail.

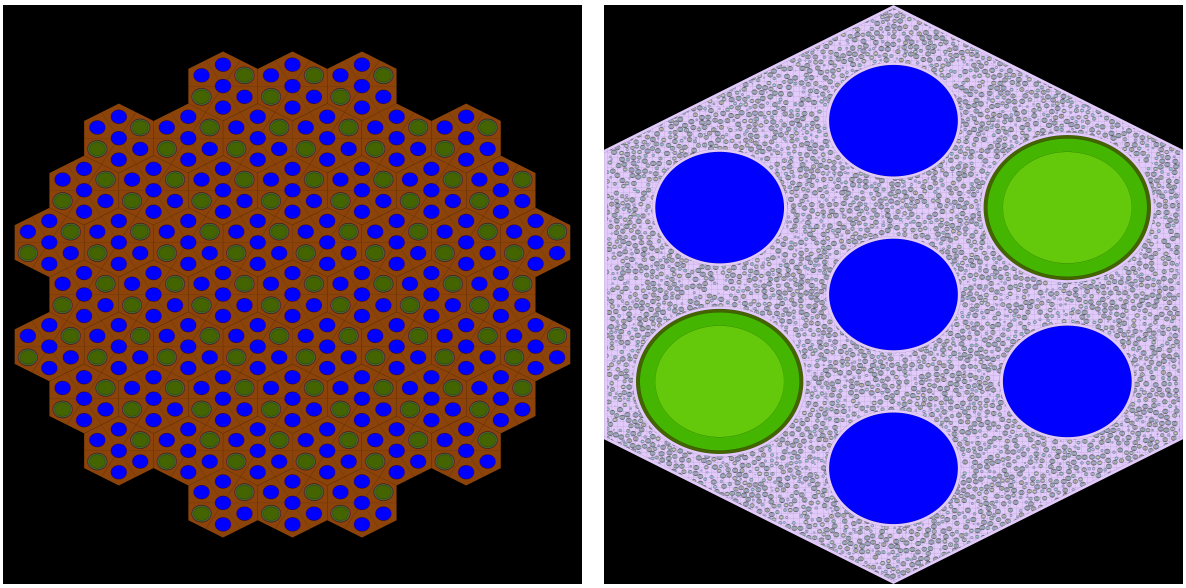

(a) Core layout on the x-y plane (b) Fuel Assembly layout on the x-y plane

Figure 3: Reactor configuration

4 Solid moderator candidates

In thermal spectrum nuclear system, the choice of the moderator is a primary driver of core size and neutronic performance and for that it needs to be accurately contextualized in an exceptional application which is the SELENE project, which presents very different characteristics from the terrestrial ones. In a compact HALEU fueled system such as the object of this study, the trade-off between the constraints and requirements presented in the previous chapter led to the decision to avoid liquid moderators. In fact, despite their widespread use in currently operating nuclear power plants, they present intrinsic challenges in the lunar environment that make them an unviable solution. In this chapter, the five main candidate materials to be used as solid moderators are presented in detail.

4.1 Criteria for selecting solid moderators

From a broad and interdisciplinary perspective, the main properties of ideal solid moderators for space applications, useful to guide the choice between different materials, can be grouped into six categories. These are as follows:

- **nuclear properties** such as high scattering cross section, low absorption cross section, low atomic mass, stability under neutron irradiation;
- **safety-related properties** such as negative moderator temperature coefficient;
- **thermo-physical properties** such as low mass density, high thermal conductivity, high heat capacity, low thermal expansion coefficient and stability at high temperature;
- **mechanical properties** such as good mechanical strength, stability under irradiation and resistance to creep and fatigue;
- **chemical and compatibility properties** such as low chemical reactivity, corrosion resistance, low production of gases or degradation products and chemical stability under irradiation;
- **manufacturing readiness** including supply chain, fabrication routes, achievable geometries, quality control.

Although all these properties are crucial and should be carefully considered during a selection phase, this work focuses specifically on the neutronic ones. From this point of view, an ideal moderator can be defined as a material which slows down the largest number of fast neutrons to thermal energies while absorbing as few as possible. Initially, to get an idea of the neutronic behaviour of different materials, it is common to refer to two parameters described theoretically in chapter 2.3 such as the slowing down power and the moderating ratio. It can be said, as rule of thumb, that a high SDP can be really valuable in reducing moderator volume and improving reactor compactness, while a large MR means low absorption cross section and, consequently, a better neutron economy in the core. At the same time, the information provided by SDP and MR is not sufficient to make the best choice for a specific system. In this regard, many other neutronic parameters must be investigated in order to understand in detail the performance of the different materials for the reactor of interest. Among them, it should be mentioned the multiplication factor, moderation ratio, neutron spectrum, axial power distribution and reactivity swing. As is well known, the most widely used solid moderators are graphite, Beryllium (Be), Beryllium oxide (BeO), Zirconium hydrides (ZrH_x) and Yttrium hydride (YH_x). Over the years, these moderators have been used in many research, propulsion and space reactors, thus ensuring a certain level of reliability in terms of overall listed performance and representing a valid set of candidates that have been extensively tested and analysed. Before proceeding to their comparison for the SELENE reactor, the main neutronic characteristics of each solid moderator will be presented below.

4.2 Beryllium (Be)

Beryllium combines a low atomic mass with a very small neutron absorption cross section, making it attractive both as a moderator and a reflector in thermal spectrum cores. Typical property tables give an estimation of $\xi \approx 0.160$, low macroscopic absorption cross section and a significantly large MR. These parameters motivate the historical use of Beryllium in research reactors and its consideration in space reactor and nuclear thermal propulsion designs, often in combination with or as an alternative to Graphite. This material, anyway, poses a significant safety concern, since its toxicity imposes strict requirements on fabrication, machining and waste handling, which tend to increase cost and complexity compared to other candidates.

Table 1: Properties of Beryllium

Parameter	**Value**	**Unit**
Atomic mass	9.0122	u
Avg. logarithmic energy decrement	0.160	-
Slowing down power	0.16	cm^{-1}
Moderating ratio	145	-
Density at room temperature	1.85	g/cm^3
Thermal conductivity	≈ 200	W/(m·K)

4.3 Beryllium Oxide (BeO)

Beryllium oxide is a high melting point ceramic with excellent thermal conductivity, structural stiffness and similar neutronic properties to metallic Beryllium. Having $\xi \approx 0.163$ and a very low thermal neutron absorption cross section for both Be and O, BeO exhibits, as a consequence, decent SDP and high MP values; for these reasons, like Be, also BeO has been widely studied as a moderator and reflector in high temperature reactors and as a candidate for space power systems. Under irradiation, however, Beryllium oxide is limited by similar problems encountered by a lot of materials: assessments of irradiated BeO have shown that microcracking and property degradation occur at a wide range of temperatures, including the rated one for SELENE reactor (1200K)

Table 2: Properties of Beryllium oxide

Parameter	**Value**	**Unit**
Molecular mass	25.0116	u
Avg. logarithmic energy decrement	0.163	-
Slowing down power	0.710	cm^{-1}
Moderating ratio	118	-
Density at room temperature	3.01	g/cm^3
Thermal conductivity	$\approx$ 250-300	W/(m·K)

4.4 Graphite (Gr)

Graphite is a classical solid moderator and remains the reference material for many non-water cooled reactor concepts, including High Temperature Gas cooled Reactors (HTGRs) and old RBMK reactors. Its main appeal lies in its extremely low neutron absorption cross section which results in a MR substantially higher than that of all the

other candidates. On the other hand, it has a modest slowing down capability and, consequently, a relatively low SDP. This implies that large volumes are required to achieve thermalization levels comparable to those obtained with other moderators. In the case of SNRs, this becomes an important disadvantage due to the strict constraints on system mass and volume. From an engineering perspective, graphite benefits from mature supply chains and extremely high melting point but suffers from embrittlement due to dpa, as well as moderate irradiation swelling.

Table 3: Properties of Graphite

Parameter	**Value**	**Unit**
Atomic mass	12.011	u
Avg. logarithmic energy decrement	0.063	-
Slowing down power	0.065	cm^{-1}
Moderating ratio	176	-
Density at room temperature	1.70-1.85	g/cm^3
Thermal conductivity	$\approx$ 100-140	W/(m·K)

4.5 Zirconium Hydride (ZrH_x)

Zirconium hydride has a long history as a neutron moderator and, in the form of U–ZrH alloys, has been used as a combined fuel–moderator in research reactors and space power systems. ZrH_x has become an attractive option because it combines a high hydrogen atom density (high scattering cross section, high ξ) with relatively low neutron absorption, yielding a very high SDP but a sensibly lower MR ($\approx$ 50) with respect to, for example, Graphite. As shown in Figure 5, zirconium hydride (ZrH_x) can exist in different crystalline phases depending on the hydrogen content x and temperature. From a neutronic point of view, the hydrogen density of the δ-phase ensures a high scattering cross section and good moderation due to a good hydrogen retention. Furthermore, this phase offers low risk of cracking, high thermal stability and reduced lattice distortion. At the operating temperature of interest for the SELENE reactor ($\approx$ 1200 K), this phase exists for a hydrogen-to-metal ratio varying approximately from 1.4 to 2.0. As a reference value, an H/Zr ratio of 1.6 has been considered. At the same time, different ratios have also been analyzed in order to assess their effect on moderation and therefore on criticality. An important issue associated with zirconium hydride is the variation in hydrogen concentration that, at high temperature and in the absence of a ad-hoc barrier,

would occur due to temperature and gradients in concentration. Hydrogen migration affects directly the moderation performance and subsequent losses make moderation less efficient. Although this phenomenon occurs at the operating temperatures of the SELENE reactor, it has been neglected in the present study. In fact, all calculations were performed considering that the density of zirconium hydride is constant at room temperature.

Table 4: Properties of Zirconium Hydride(1.6)

Parameter	**Value**	**Unit**
Molecular mass	93.03	u
Avg. logarithmic energy decrement	1.540	-
Slowing down power	1.53	cm^{-1}
Moderating ratio	51	-
Density at room temperature	5.65	g/cm^3
Thermal conductivity	$\approx$ 17-20	W/(m·K)

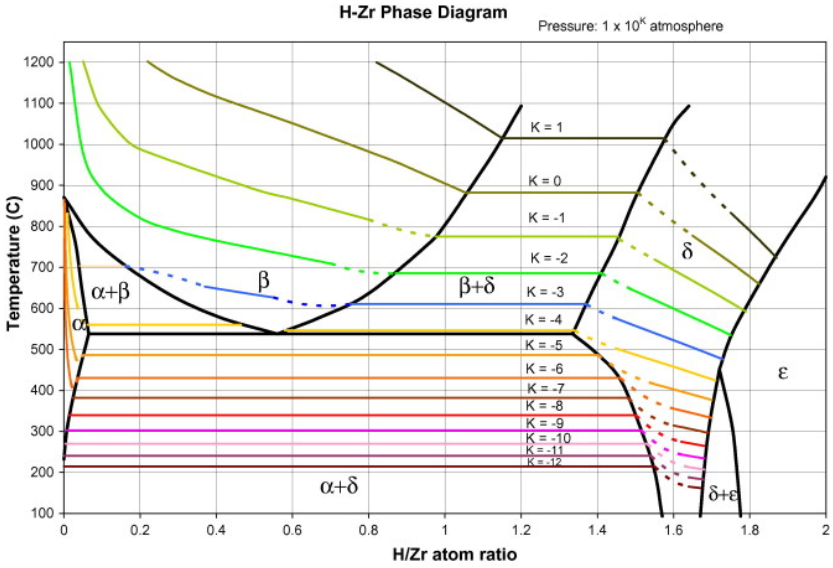

Figure 4: H-Zr phase diagram, Doonyapong (2010)

4.6 Yttrium Hydride (YH_x)

Yttrium hydride has established itself as a promising solid neutron moderator as it offers a good combination of high SDP alongside acceptably low neutron absorption cross section of yttrium, resulting in robust scattering properties but a comparatively modest moderating ratio ($\approx$ 25). As in the case of ZrH_x, the stoichiometric hydrogen-to-metal

ratio plays a fundamental role and the objective is to remain within the δ-phase. As showed in the Y-H phase diagram in Figure 5, the δ-phase of this material spans roughly the interval 1.5-1.9, depending on the operative temperature. The configuration chosen as a reference is $YH_{1.85}$. Its somewhat poorer moderating parameters compared to $ZrH_{1.6}$, can often be neglected by the benefits of higher allowable operating temperature and very good high-temperature hydrogen retention. As discussed above for ZrH_x, variations in hydrogen concentration caused by concentration and temperature gradients are neglected in the present work.

Table 5: Properties of Yttrium Hydride(1.85)).

Parameter	**Value**	**Unit**
Molecular mass	90.61	u
Avg. logarithmic energy decrement	$\approx$ 1.200	-
Slowing down power	$\approx$ 1.2	cm^{-1}
Moderating ratio	25	-
Density at room temperature	4.30	g/cm^3
Thermal conductivity	$\approx$ 20-25	W/(m·K)

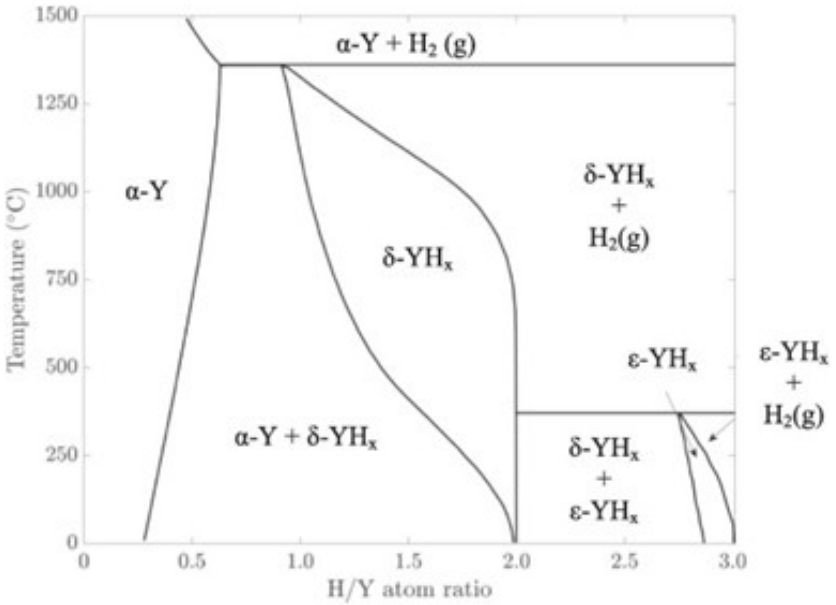

Figure 5: H-Y phase diagram, Jordan (2025)

5 Methodology

This chapter outlines the computational approaches employed for the neutronics analysis in this thesis, with a focus on the approaches chosen to tackle each phenomenon and to get consistent results based on coherent assumptions. The methodology is based on the Serpent Monte Carlo code as the neutron transport solver, whose main features will be given an introduction to, then, will follow an assessment of the principal characteristics that all the simulations of this work have in common (TRISO fuel modeling, boundary conditions and limitations inherent to FA-level analyses). In conclusion, for each set of obtained results, a connection will be made between the theoretical background, Serpent code adaptation and the presented results.

5.1 The Serpent Monte Carlo code

Serpent is a continuous-energy Monte Carlo particle transport code designed primarily for neutron and photon simulations in nuclear reactor physics. At its core, the Monte Carlo methodology in Serpent relies on statistical sampling of particle histories: individual neutrons (or photons) are tracked through the simulated geometry, with their interactions such as scattering, absorption, fission or leakage governed by probability distributions derived from evaluated nuclear data libraries in ACE format (e.g., ENDF/B, JEFF, JENDL). This analog or variance-reduced tracking mimics real physical processes without spatial or energy discretization, enabling unbiased estimation of quantities like effective multiplication factor (k_{eff}), reaction rates, fluxes, and pin powers directly from tallying collision densities or track-length estimators across billions of simulated histories. Integrated within the Kraken multi-physics framework, Serpent serves dual roles: as a high fidelity reference solver for full core analyses with explicit 3D geometries, or as a lattice physics tool generating homogenized multigroup constants [13]. In this thesis, Serpent 2.2.1 is employed to model the detailed FA geometry with continuous-energy cross sections ensuring methodological consistency between reference Monte Carlo benchmarks and assembly level simulations.

5.2 Modeling approaches of the TRISO-type fuel

As already presented in various circumstances, the design choice for the fuel of SELENE reactor has been assigned to TRISO particles immersed in a SiC matrix with a packing fraction of 40%; due to the stochastic nature of this fuel, its modelling in a Monte Carlo code can take different ways. In this work, two alternative modeling approaches were tested in order to compare their effects on the neutronic parameters and are as follows:

- an explicit modeling of the TRISO particles, where their random distribution is simulated
- an homogeneous modeling, where TRISO particles and SiC matrix are treated as a single, homogeneous material

It should be noted that this two approaches differ only in modeling the fuel region, every other FA region being the same. Although the homogeneous approach can be extremely useful, being computationally lighter and more easily implemented, from a physical point of view, it has an important effect. Indeed, with a homogeneous description, the resonance escape probability (p) i.e., the probability that neutrons escape capture during slowing down, is reduced compared to the explicit case, resulting in an underestimation of the criticality of the system. This is due to the fact that the main absorber, $U-238$, which in the real case is confined within the TRISO kernel (i.e., the most internal layer of the particle), is instead uniformly distributed throughout the fuel compact region in the homogeneous description, causing a reduction of the resonance self-shielding of the fuel. Serpent allows for the explicit modeling of this type of fuel through a dedicated card ('pbed') in which materials and dimensions of the particle layers can be set, as shown in Figure 6. Furthermore, a dedicated software routine ('disp') provides a stochastic 3D distribution of each TRISO particle as a function of FA shape and packing fraction. In the context of the present work, the homogeneous modeling is performed according to the volume-weighted homogenization (VWH) method, a technique that requires the definition of an ad hoc mixture that preserves the volumes of all materials. This was implemented by defining a single material with adequate atomic fractions, as shown in Table 13.

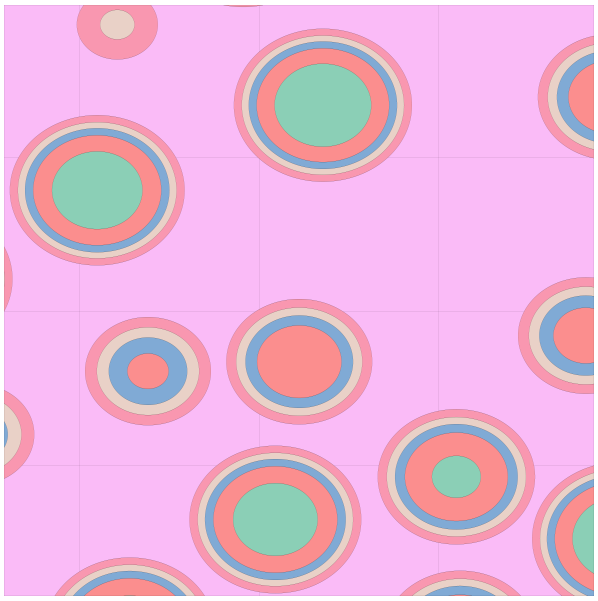

Figure 6: Serpent TRISO pebbles close up

A comparison of these approaches was presented in the first section of the result chapter (6.1), where the k_∞ values of the two configurations were analyzed.

5.3 Boundary conditions and limitations of the fuel assembly analysis

As discussed in chapter 3, the SELENE reactor configuration considered in this work is preliminary and incomplete. It includes 55 fuel assemblies in order to ensure the required power over 10 years, but control and shutdown systems and neutron reflector are not yet included. Therefore, it seemed reasonable to limit the analyses to the fuel assembly level. This level of analysis is adequate to evaluate the performance differences among the five solid moderators in order to orient the subsequent design phases. To do this, the reflective boundary conditions along both the axial and radial directions were imposed (except for the analyses regarding the axial power distribution, for which the axial reflective boundary condition was removed). It is worth noting that, by treating the fuel assembly boundaries as perfectly reflecting, the simulation represents a radially and axially infinite lattice of identical assemblies, which accurately represents the behaviour of a generic FA in the middle (or far enough from the boundaries) of the SELENE core. Consequently, the infinite multiplication factor (k_∞) is calculated, which provides a high-fidelity characterization of the fuel's intrinsic neutronic performance and resonance self shielding. At the same time, this level of analysis implies some important limitations due to the fact that the neutron leakage is neglected. In fact, when moving

to the full-core level, most neutronic parameters such as criticality at BOL and EOL, spectrum, power distributions and reactivity swing must be recalculated.

5.4 Neutronic simulation setup

Having introduced the two main features of all the analyses presented in the Results chapter, it is now fundamental to dive into the neutronic simulations setup to give a clear understanding of the key elements of each of the numerous simulations. In this paragraph will be given the common tools that need to set for each typical Serpent run, before detailing what was added or modified for each specific scope in the next subsections. To establish a high-fidelity neutronic model in Serpent, the input file is structured into several functional blocks that define the nuclear data, materials, geometry, and simulation controls. The model is based on the nuclear data libraries, in which continuous-energy interaction data in ACE format are linked inside the script. ENDF/B-VIII.0 were the ones chosen for this work [2]. A specific mention is needed for thermal scattering data, $S(\alpha, \beta)$, which, as explained in paragraph 2.4, are the necessary tool to accurately model the thermalization process (under the threshold of E_{cutoff}) where precise data regarding target nuclei motion are needed. This functionality is activated through the 'moder' card. The geometry is then built following Serpent's universe-based model where boundary surface are defined ('surf'), to be occupied by cells ('cell') which, in turn, are filled with the materials ('mat'). The other essential simulation parameters are 'set pop' and the already discussed 'set bc': the first card controls the statistics of the simulation since it needs the numbers of neutrons per cycle, the number of active cycles (≈ 200) and the number of inactive cycles (≈ 160).

5.4.1 Moderation curve

The analysis of how a change in the amount of moderator affects the criticality of the system is a key aspect from a neutronic point of view. In the literature, two different approaches can be found for this purpose: the moderation ratio [19] and the moderator-to-fuel ratio. While the former is defined in terms of the ratio of volumes (generally, moderator to fuel, V_m/V_f), the latter is based on the ratio of atomic densities (N_m/N_f). Although at first glance they seem to provide the same result, a more in-depth analysis reveals a not completely negligible difference. This is due to the fact that, if in the moderation ratio analysis the density is kept fixed while the geometry is modified in order to vary the amount of moderator in the system, in the moderator-to-fuel ratio analysis the opposite approach is used. This means, in other words, that in the two cases a certain amount of mass is arranged differently, resulting in a difference in criticality that becomes more significant as the difference between two arrangements increases. This discussion suggests that the first analysis should be used to evaluate the optimum of moderation within the reactor design framework, while the second analysis is more appropriate for safety-related calculations such as those related to moderator reactivity coefficients. According to the general goal of this work, a moderation ratio analysis was performed. Operationally, the moderation ratio curve was derived from 14 different configurations (including the smallest and the largest shown in Figures 7a and 7b) obtained by gradually increasing the radius of the moderator pins.

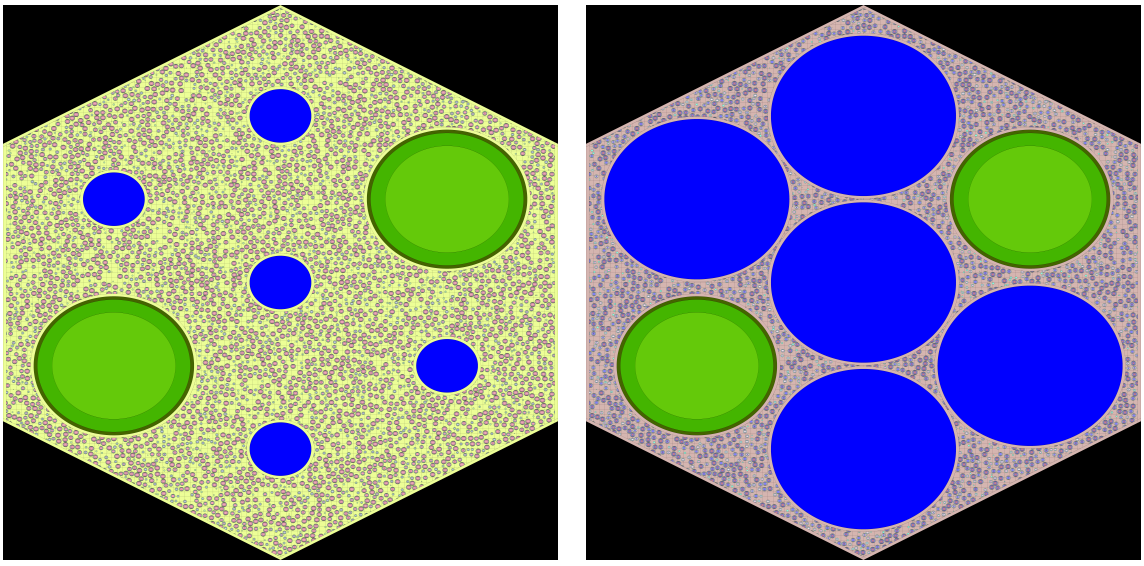

(a) Minimum V_{mod} (b) Maximum V_{mod}

Figure 7: Limit configurations

5.4.2 Spectra plots

To generate a spectrum plot, two elements are necessary: a detector card for the selected universe (or cell) and an appropriate energy grid. For each chosen configuration, it was deemed reasonable to analyze the neutron flux spectrum along the whole FA to better appreciate the moderator's overall impact on the domain physics, thus activating in each analyzed configuration a dedicated 'det' card. For what concerns the energy binning, the SHEM 281 energy group structure was chosen [22] (Table 24 in Appendix A). The generated detector tallies, for each configuration, were multiplied by the source rate to obtain the lethargy-normalized neutron spectrum, which was plotted for each moderator for three different values of the moderation ratio.

5.4.3 Group constants generation

A set of important calculations is the one that regards group constants generation. In the framework of this thesis, the needed parameters are absorption and scattering cross sections which, in turn, are fundamental to compare the purely neutronic performance of each moderator through the slowing down power and the moderating ratio. The Serpent code is characterized by a very specific functionality that allows obtaining group constants, homogenized in space and energy Σ_s and Σ_a, tailored for a specific application. To do so, Serpent utilizes its in-built routines to define appropriate collision estimators which provide the corresponding reaction rate tally; then, these reaction rates are automatically homogenized on the corresponding energy group and selected universe volume, and finally, normalized on the scalar flux. The theoretical approach utilized to obtain a scattering cross is shown below:

$$\Sigma_{s,EE'} = \frac{\int_V \int_{\Delta E} \int_{\Delta E'} \Sigma_s(r, E \rightarrow E') \; \phi(r, E) \; dE dE' dV}{\int_V \int_{\Delta E} \phi(r, E) \; dE dV} \tag{14}$$

Having chosen the moderator universe as the volume on which normalizing (card 'set gcu'), a 2-group energy grid, with thermal cut off of $0.625eV$, the final output was obtained and later utilized for the SDP and MR calculations.

5.4.4 Changing hydrogen-to-metal ratio

As discussed in paragraphs 4.5 and 4.6, the hydrogen-to-metal ratio has huge implications in terms of compound phase and indirectly, neutronics. To understand how this

ratio impacts the k_∞in the configurations using metal hydrides, the stability range of the δ-phase was chosen and so the corresponding atomic fractions and densities had to be reevaluate for each value. The density correlations, expressed as a function of the hydrogen-to-metal atomic ratio for ZrH_x and YH_x, are the following and come from [28], [7]

$$\rho = \begin{cases} 1/(0.1541 + 0.0145(H/Zr))) & \text{for } H/Zr < 1.6 \\ 1/(0.1706 + 0.0042(H/Zr)) & \text{for } H/Zr \geq 1.6 \end{cases} \tag{15}$$

$$\rho = 4.37 - (H/Y) \ \cdot 5.82 \ \cdot 10^{-2} \tag{16}$$

After having found the new densities, the final step was to calculate the new atomic fractions, which were obtained by proportion utilizing the original values for the $ZrH_{1.6}$ and $YH_{1.85}$ configurations.

5.4.5 Axial linear power density

One of the goal of this comparison was to assess the effects of the different moderators on the axial power distribution. For this purpose linear power density calculations were performed. In Serpent, this was done by defining a fission power detector along the axial length of the FA (with a space binning of 100 intervals). The adopted strategy is divided into two steps:

- first, the linear power density of each configuration was analyzed under reflective boundary conditions in order to assess how it is influenced by the different moderation ratios (V_m/V_f), each corresponding to the maximum moderation of that configuration;
- second, the axial linear power density profiles are evaluated for the same configuration (i.e., for a fixed moderation ratio) without the reflective boundary condition along the z direction. For this analysis, two 30 cm layers of BeO reflector were placed at the ends of the FA. As shown in Figures 8a and 8b, although the upper and lower reflectors have the same thickness, the upper reflector does not cover the entire surface due to the presence of two cylindrical channels left empty to accommodate the extension of the heat pipes reaching the outer HRS.

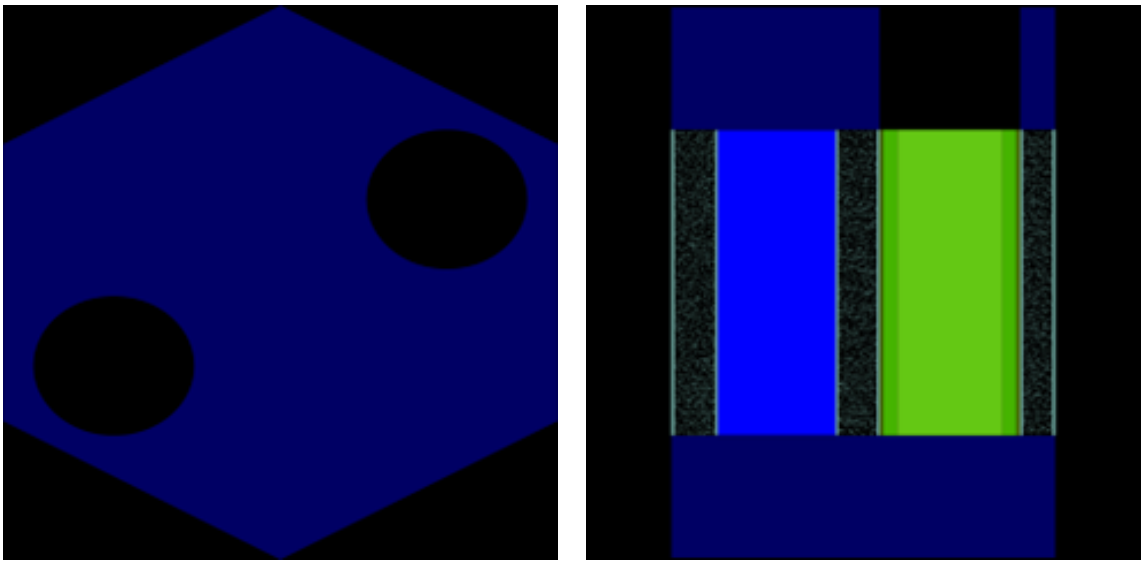

(a) top view of upper reflector layer (b) side view of the FA

Figure 8: BeO reflector positioning

5.4.6 Burnup calculations

The depletion calculations were performed for each moderator configuration considering a power of 9.0909 kW (1/55 of the nominal thermal power of 500 kW) and an availability factor of 100%. The specifics here, concern the additional inputs that are needed to run correct burnup simulations:

- 'burn' card, to be associated with the burnable material (i.e., TRISO kernel);
- 'dep' card, where the time steps for the analysis must be specified. To account for the physical phenomena typical of thermal spectrum reactors, 26 time steps were considered. These are reported in Table 23 in Appendix A.
- depletion libraries, which are specific datasets that allow Serpent to calculate how the material composition of a nuclear reactor changes over time due to irradiation in terms of radioactive decay, transmutation and other processed. In accordance with the nuclear data library used, the depletion data comes from ENDF/B-VIII.0.

.

6 Results

6.1 Moderation ratios and optimum moderation conditions

The first assessment of the neutronic performance of these materials begins by analysing how the variation of the ratio between the moderator volume and the fuel volume, i.e., V_{mod}/V_{fuel}, referred from now on as moderation ratio, impacts the multiplication factor of the FA. Having fixed the positions of both the two heat pipes and the moderator pins, the dimensions of the cell and the TRISO distribution, the only geometric variable left to modify the moderation ratio is the diameter of the moderator pins. The boundary values were obtained by choosing an arbitrary minimum radius of 0.5 cm and a maximum of 1.5 cm, which avoids superposition between the different components as shown in Figures 7a and 7b in paragraph 5.4.1. It is also important to note from these graphs that, given that every other component is fixed, changing the dimension of the moderator pins impacts not only the numerator of the MR, but also V_{fuel}, making it particularly important to investigate this matter.

The calculations, for this section only, were also portrayed for the homogeneous fuel configuration to directly compare the hypothesis and comments made in paragraph 5.3; therefore, below in Figure 16, can be found the moderator curves evaluated for each material in both the homogeneous and explicit configurations.

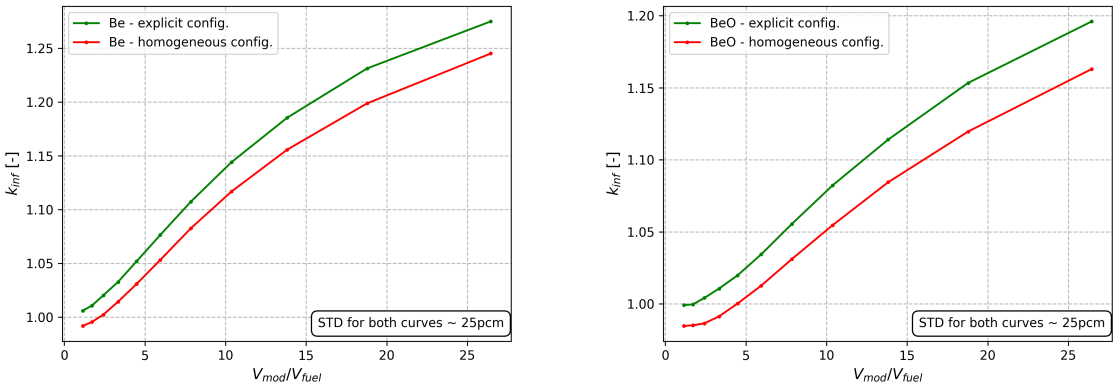

(a) Be (b) BeO

Figure 9: k_∞ as a function of the moderation ratio for both homogeneous and explicit configurations **(1/2)**

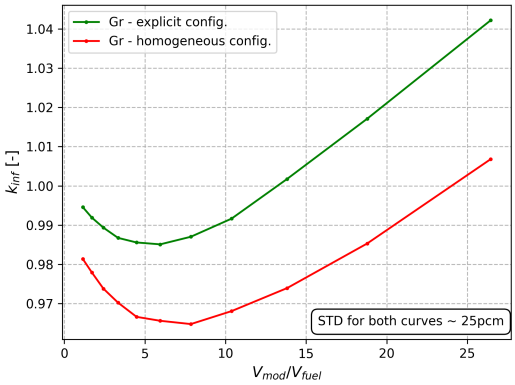

(c) Graphite

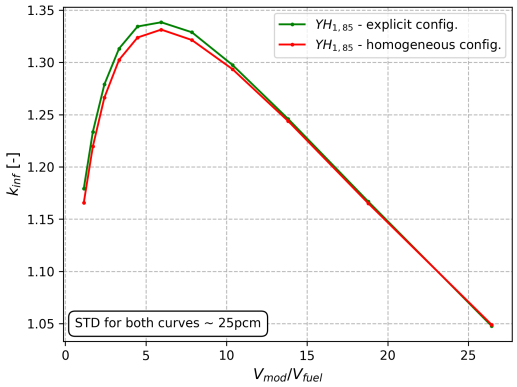

(d) $YH_{1.85}$

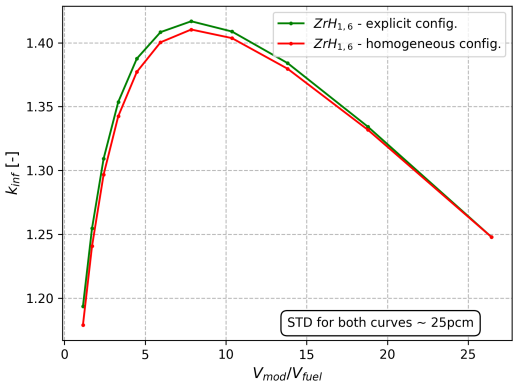

(e) $ZrH_{1.6}$

Figure 9: k_∞ as a function of the moderation ratio for both homogeneous and explicit configurations **(2/2)**

The first consideration to make is the significant difference between the two different fuel formulations: as expected, all the homogeneous configurations end up underestimating the k_∞ by a significant amount (up to a $\Delta k = 3561 pcm$ for the Graphite plot), as reported in Table 6. Another striking difference is found between the hydride graphs, Figures 9e, 9d and the other three; in the trends for $ZrH_{1.6}$ and $YH_{1.85}$, the optimum configuration can be easily found as well as the over and under moderated regions that lie to the right and to the left of the curve maximum, respectively. Be and BeO configurations, in Figures 9a, 9b, on the other hand, present a monotonic profile that increases until the maximum value of moderation ratio, thus highlighting that all explored configurations are in under moderated conditions; which is partially true also for the Graphite plot, in Figure 9c, where, the trend, before increasing along with the moderation ratio, present a slight dip for the six smallest moderator configurations.

This behaviour is justified by the material characteristics discussed in chapter 4, because the counterintuitive value of k_∞ that decreases with increasing moderator volume is due to Graphite's particularly low SDP, whose effect becomes relevant only when a significant amount of moderator volume is inserted, in this case for MR = 5.95.

Table 6 reports the condensed data highlighting the highest registered value of k_∞ at corresponding moderation ratio; it is clear that, with a $k_\infty = 1.41625$, $ZrH_{1.6}$ confirms its exceptional slowing down properties ($V_{mod}/V_{fuel} = 7.85$). Similar considerations can be made for $YH_{1.85}$, which has its optimum configuration with $V_{mod}/V_{fuel} = 5.95$ and a slightly lower value of k_∞. For what concerns the other three materials, as written previously, they all exhibit the highest multiplication factor for the configuration with the highest moderation ratio (26.45), hence confirming the expected consequence of a lower ξ, with Graphite reaching the lowest overall value of k_∞.

Table 6: Optimized k_∞ configurations

Moderator	V_m $[\frac{g}{cm^3}]$	V_f $[\frac{g}{cm^3}]$	V_m/V_f [-]	k_∞, **expl.**	k_∞, **homog.**	Δk [pcm]
Be	2650.7	332.47	26.45	1.27617	1.24506	3561
BeO	2650.7	332.47	26.45	1.19678	1.16296	3382
Graphite	2650.7	332.47	26.45	1.04104	1.00681	3423
$ZrH_{1.6}$	1425.5	1557.67	7.85	1.41621	1.41040	581
$YH_{1.85}$	1176.5	1806.67	5.95	1.33919	1.33139	780

As expected, the harder the spectrum (due to a less efficient moderation), the greater the difference between the explicit and homogeneous configurations. Indeed, as the spectrum hardens, the probability that a neutron escapes resonance absorption is significantly lower in the homogeneous configuration than in the explicit one.

6.2 Spectrum and spectral index in under moderated, optimum moderated and over moderated conditions

A coherent follow-up to the evaluation of the moderation curves that have just been analysed, is the analysis of the neutronic flux spectra and the related spectral indexes (SI). The neutron spectrum represents the distribution of the flux as a function of the energy, allowing for significant comparisons in terms of moderator effectiveness and its general impact on the reactor physics. For each chosen moderator, the flux was evaluated for three different values of moderation ratios to better appreciate the discrepancies between the different regions of the moderator curves. Taking these as a reference, the chosen methodology is the following: for the hydrides it was simple to select (other than the optimum configuration) the under and over moderated configurations corresponding to the geometries with the lowest and highest possible moderation ratios, respectively. For what concerns Be, BeO and Graphite, as seen before in paragraph 6.1, all possible V_{mod}/V_{fuel} configurations instead will represent an under moderated one, thus the three investigated below.

As said in 5.4.2, the spectra plots presented in Figure 10 are obtained for the whole FA. The detector tallies were multiplied by the source rate to finally obtain the lethargy-normalized neutron spectrum.

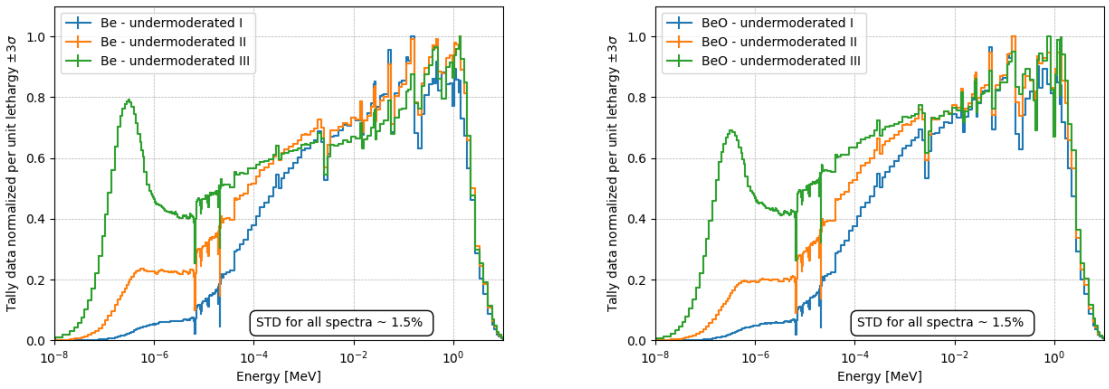

(a) Be (b) BeO

Figure 10: Neutronic flux spectra evaluated for three configurations **(1/2)**

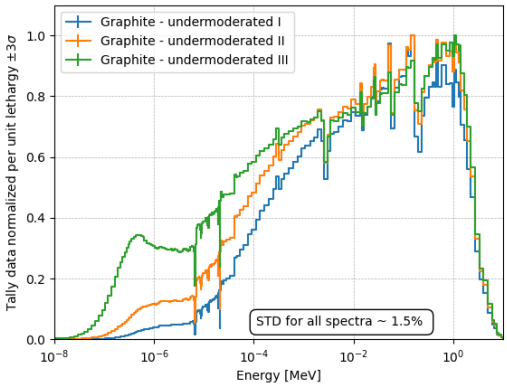

(c) Graphite

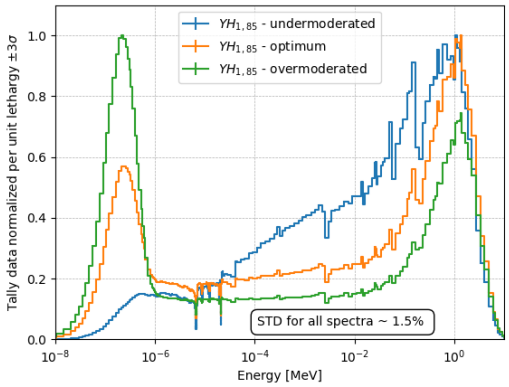

(d) $YH_{1.85}$

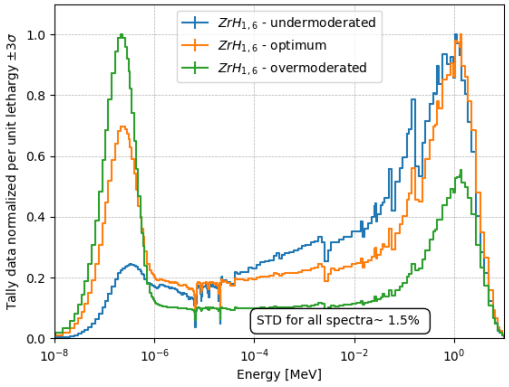

(e) $ZrH_{1.6}$

Figure 10: Neutronic flux spectra evaluated for three configurations **(2/2)**

The first characteristic that immediately shows up is, again, the similarity between the profiles of the two hydrides and among the other three moderators. Starting from the latter, Be (Figure 10a), BeO (Figure 10b) and Graphite (Figure 10c), it is evident that all spectra have a very pronounced fast peak with a significant epithermal tail ending with a relatively flat thermal region, meaning a hard spectrum for each configuration. The 'softest' spectra are registered, as expected, in the 'under moderated III' configurations, which correspond to those with the highest k_∞ value. Furthermore, comparing these data with the moderation ratio curves, it can be notes that Be exhibits the more balanced spectra and the highest k_∞ value, while the opposite is observed for Graphite. Moving to the hydrides spectra, found in figures 10d and 10e, it can be observed that the pronounced green spikes in the thermal region truthfully represent the typical behaviour of an over moderated system. In fact, this system is characterized by too many moderator absorptions over fuel absorptions due to the excessively

value of moderation ratio: the result is an excessive number of 'unusable' neutrons in the thermal range and a very soft spectrum. On the contrary, the blue profile, which represents the under moderated configurations, is also consistent: a small moderator volume determines an insufficient slowing down, resulting in a weak thermal flux and a large epithermal tail, particularly evident in YH. Both optimum configurations return, as expected, an equilibrium between the other two trends, meaning that the neutron population is correctly managed.

A useful parameter to evaluate a neutron flux spectrum and assess the moderator performance is through the spectral index. This is defined as the ratio of neutron reaction rates or flux components in different energy ranges, and is used to characterise the shape (hardness or softness) of the neutron energy spectrum in a reactor. In this work, the spectral index is taken as the ratio of the maximum flux in the fast region and the maximum flux in the thermal region, as shown in the following equation:

$$SI = \frac{\Phi_{fast}}{\Phi_{th}} \tag{17}$$

The computed values for each spectrum are found, for the hydrides in Table 7, and for Be, BeO and Graphite in Table 8.

Table 7: Operating conditions, moderation ratio (V_m/V_f) and spectral index: $ZrH_{1.6}$, $YH_{1.85}$

Condition	V_m/V_f [-]		Spectral index [-]	
	$ZrH_{1.6}$	$YH_{1.85}$	$ZrH_{1.6}$	$YH_{1.85}$
Optimum	7.85	5.95	1.86	2.24
Undermoderated	1.15	1.15	4.33	14.3
Overmoderated	26.45	26.45	1.02	0.96

Table 8: Operating conditions, moderation ratio (V_m/V_f) and spectral index: Be, BeO, Graphite

Condition	V_m/V_f [-]			Spectral index [-]		
	Be	BeO	Gr	Be	BeO	Gr
Undermoderated I	1.15	1.15	1.15	23.9	31.5	27.2
Undermoderated II	5.95	5.95	5.95	7.12	7.13	18.9
Undermoderated III	26.45	26.45	26.45	1.69	2.20	4.78

As mentioned above, the very hard spectra exhibited by Be, BeO and Graphite are confirmed by the SI calculated for the under moderated configurations I, II, with the highest value (31.5) observed for beryllium oxide. This shows also for for the under moderated $YH_{1.85}$, which has a significantly hard spectrum with an SI of 14,3. An opposite behaviour has been highlighted for the soft over moderated spectra, which, in fact, result in very low SI values (0.96 for $YH_{1.85}$ and 1.02 for $ZrH_{1.6}$). Finally, it is particularly interesting to observe that the SI values for both the optimal hydride configurations and the under moderated configuration (III) of Be and BeO fall within the range [1.69, 2.24], making them directly comparable in terms of neutron flux distribution.

6.3 Cross sections, slowing-down powers, moderating ratios

The next important set of calculations that were done, regards the slowing down powers and moderating ratios of each material. As discussed in the chapter on the theoretical background, these parameters are useful indicators for a preliminary assessment of moderator performance. The goal of this section is to calculate these parameters for the system under consideration. For this reason, the specific effective microscopic cross sections of the SELENE reactor were used. The SDP and MR values thus obtained are reported in Table 9.

Table 9: Evaluated moderator parameters

				calculated		**from literature**	
	ξ [-]	Σ_c [cm^{-1}]	Σ_s [cm^{-1}]	SDP [cm^{-1}]	MR [-]	SDP [cm^{-1}]	MR [-]
$ZrH_{1.6}$	1.54	3.18×10^{-2}	1.113	1.713	54	1.530	51
$YH_{1.85}$	1.20	2.93×10^{-2}	0.945	1.134	39	1.200	25
BeO	0.16	1.12×10^{-2}	0.622	0.102	91	0.710	118
Be	0.16	8.01×10^{-4}	0.656	0.105	131	0.160	145
Graphite	0.06	2.02×10^{-4}	0.611	0.038	188	0.065	176

Comparing the calculated values with those from literature [26], it can be noted that these two parameters depend weakly on the peculiar spectral conditions of the SELENE FA. Graphite is confirmed to be the most efficient moderator in terms of MR and, at the same time, the least efficient in terms of SDP, with a value an order of magnitude less than the other materials. The relatively high capture cross sections of the hydrides lead to them having a sensibly lower MR; at the same time, larger Σ_s values result in larger SDPs, as it was shown in both well-balanced spectra of the optimum configurations. Finally, both Be and BeO exhibit intermediate values between the previous ones, showing anyway scattering cross sections comparable with that of graphite, but with a higher ξ and, consequently, a slightly higher slowing-down power.

6.4 Effects of the H/metal ratio in the metal hydrides on the FA criticality

In this section, the discussion is focused on the metal hydrides in order to analyze how variations in the atomic ratios between hydrogen and metal affect their neutronic performance in terms of the multiplication factor. The favorable moderation properties of hydrogen are well known and have already discussed in the previous chapters: having an atomic mass approximately equal to that of a neutron, it simultaneously ensures a quite high scattering cross section and a relatively low absorption cross section; moreover, as shown in chapter 3.1, molecular hydrogen provides the biggest possible value of energy loss per collision. As a consequence, chemicals such as ZrH_x and YH_x, which have a very high hydrogen density, ensure a large number of scattering centers per unit volume, leading to the good moderation values. Taking into account these premises, it is of high interest to investigate how much positive reactivity can be inserted by modifying the hydrogen-to-metal ratio.

It is important to note that those concentration variations cannot be chosen arbitrarily. In fact, as shown in the paragraphs 4.5 and 4.6, it is fundamental to check the phase diagrams to find the range of atomic ratios that allows the compound to remain in the δ-phase. At an operating temperature of 1200K, this range varies approximately from 1.4 to 2 for zirconium hydride and from 1.5 to 1.9 for yttrium hydride. The densities and atomic fractions were adjusted consistently for each configuration (as explained in section 5.4.4). The results thus obtained are shown in Figures 11a, and 11b, while a detailed summary is also provided in Tables 10 and 11.

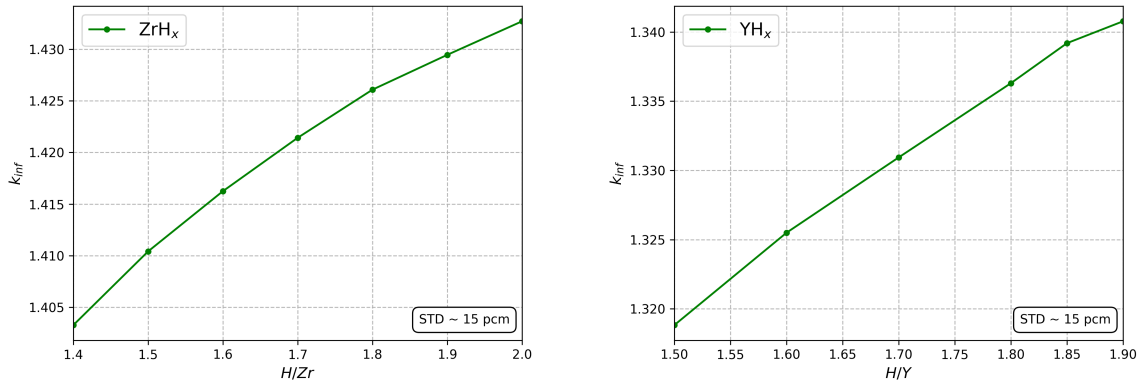

(a) ZrH_x (b) YH_x

Figure 11: k_∞ as a function of hydrogen-to-metal ratio

Table 10: Density (ρ) and k_∞ with different H/Zr ratio

ZrH							
H/Zr	1.4	1.5	1.6	1.7	1.8	1.9	2.0
ρ	5.44722	5.40233	5.35815	5.31468	5.27192	5.22983	5.18842
k_∞	1.40328	1.41042	1.41625	1.42142	1.42608	1.42945	1.43270

Table 11: Density (ρ) and k_∞ with different H/Y ratio

YH						
H/Y	1.5	1.6	1.7	1.8	1.85	1.9
ρ	4.2613	4.2555	4.2497	4.2439	4.2400	4.2381
k_∞	1.31883	1.32550	1.33094	1.33630	1.33919	1.34077

The most important takeaway is that, as expected, by increasing the atomic fraction of hydrogen also the k_∞ increases. For both ZrH_x and YH_x, the trend is approximately linear and reaches the maximum multiplication factor value when the ratio is maximum. This occurs foe $ZrH_{2,0}$ and $YH_{1,9}$, which represent the limits of the δ-phase range for each hydride. Another interesting evaluation is the total positive reactivity variations (Δk) from the lowest to highest ratios which is $\Delta k = 2942$pcm for Zirconium hydride and $\Delta k = 2194$pcm for Yttrium hydride.

6.5 Moderator effects on the FA axial power distribution

The following section is devoted to a further comparative analysis between the five moderators. We first evaluated the effect of the moderators on FA axial power distribution for each configuration, and then repeated the procedure with an appropriate reflector replacing the axial reflective boundary conditions. This strategy aims, on one hand, to compare the different moderator profiles for the two configurations considered (one for metal hydrides and one for Be, BeO and graphite), and, on the other hand, to evaluate the differences due to the introduction of a neutron reflector.

As a starting point, the linear power density was calculated for each moderator under axial reflective boundary conditions, as shown in Figure 12; the FA configurations are taken from the Table 6, where the optimized moderation ratio was set for all subsequent analysis.

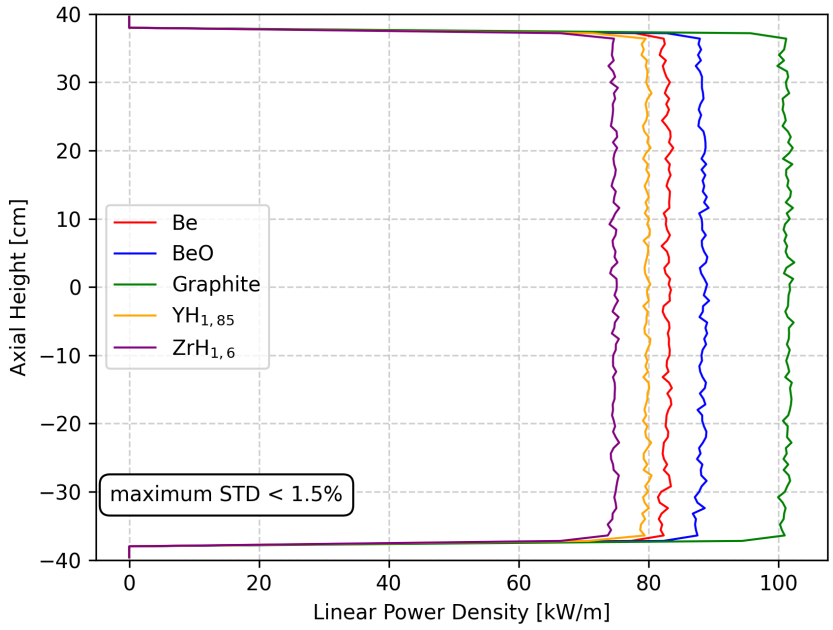

Figure 12: Linear power density without reflector

As expected, due to reflective B.C., all curves exhibit a basically flat profile along the entire length of the FA, while differing in the power density magnitude. The graphite configuration yields the highest value of $\approx$ 102kW/m, while the other materials are attested in the range $[76kW/m, 86kW/m]$, with the two hydrides being the last two. These results are consistent with the different geometrical configurations considered. Having fixed the rated power of each FA at 9.0909 kW (P_{th}/n_{ass}), the linear power

density varies with the amount of fuel present in each configuration: Graphite registers the highest value due the significantly lower V_{fuel} with respect to the hydrides; in fact, if a smaller amount of fuel has to produce the same level of power, the linear power has to be higher.

The second phase of the analysis shows the impact, on the same geometrical configurations, of two layers of a neutron reflector of BeO placed at the ends of the FA as discussed in Section 5.4.5. From the neutronic point of view, it is a fundamental addition since, as discussed in Section 5.4.5, the boundary conditions in the axial direction change and become black. It is important to analyze the results obtained in this context, since the reflector was not part of the baseline configuration, although it will certainly be included in the future. The power density profiles are shown in Figure 13:

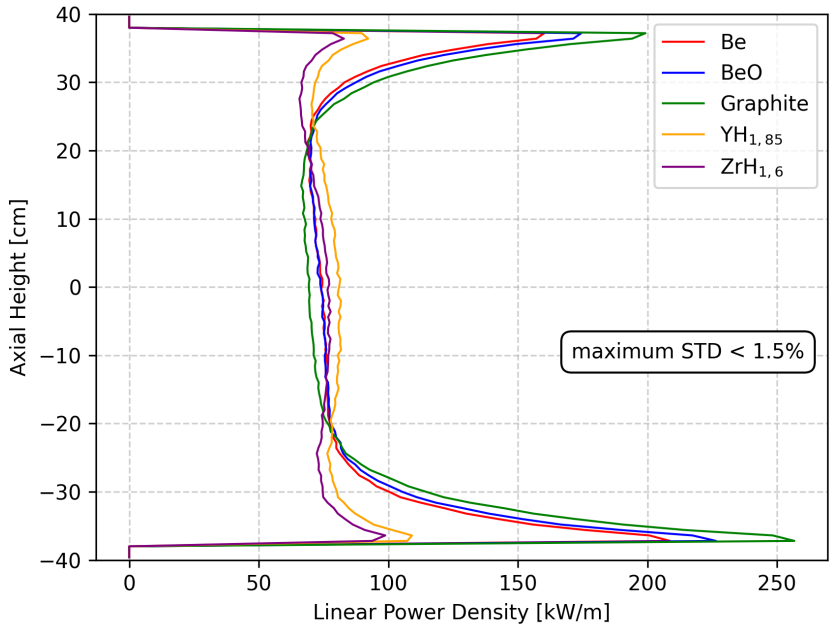

Figure 13: Linear power density with reflector

Some important differences compared to Figure 12 immediately appear: the prominent power peaks near the active length boundaries are the result of the reflector insertion, since in these configurations the neutron distribution changes drastically, accumulating near both ends of the FA. Remembering that in the upper region the reflector is perforated, more leakage is expected, and consequentely, lower power values compared to the bottom region. The graphite configuration again exhibits the highest power peak values, with $P_z(z = 37.5cm) \approx 200$kW/m and $P_z(z = -37.5cm) \approx 254$kW/m. Similar considerations with respect to the previous plot can be made, although here

are portrayed in a different way: the hydrides, which performed worse previously, again present the lowest power peaks at the boundaries, while showing a slightly higher profile in the central part of the active length. This behaviour is justified by their better slowing-down properties: since the neutron population gradient moves away from the center, a more efficient moderator is required to thermalize the neutrons in that region.

6.6 Moderator effects on the FA depletion calculations

The last section of the results is dedicated to the analysis and comparison of each moderator effect in depletion calculations over a 10-year perdiod, corresponding to the reactor expected life as defined by the SELENE operability requirements. This specific comparison between the solid moderators is particularly important because, until this point, all the calculations have been performed at Beginning Of Life (BOL) and many takeaways can be obtained from the burnup data. The evolution of the k_∞ over the 10 years of operation, considering the optimized configurations of Table 6, is showed below in Figure 14; in Appendix B are found the graphs for each single moderator (Figures 16a, 16b, 16c, 16d and 16e).

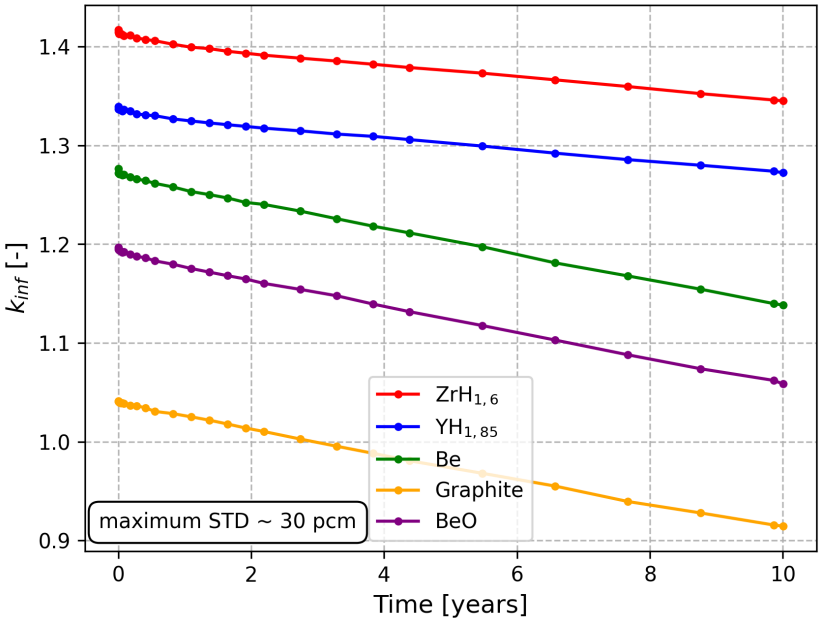

Figure 14: k_∞ as a function of time

The main observation to make from these graphs is the reactivity swing (Δk) of each moderator: $ZrH_{1.6}$ and $YH_{1.85}$ registered similar values of $\approx$ 7000 pcm, while the other 3 materials registered $\approx$ 13000 pcm. It should be noted that the graphite configuration exceeds the criticality value of k = 1 after only around three years of operation. In general, the trend for each material appears approximately linear after 2 years, while it decreases more sharply during the first months of operation. In Table 12, the most significant and useful data to compare the depletion calculations as a whole are reported, remembering that each BOL parameter is taken from Table 6.

Table 12: Resume of burnup calculations

	$k_{\infty,BOL}$	$k_{\infty,EOL}$	Δk_∞ [pcm]	Burnup $\left[\frac{\text{MWd}}{\text{kg}}\right]$	$m_{U,BOL}$ [g]	$m_{U,EOL}$ [g]	Δm_U [g]
$ZrH_{1.6}$	1.41621	1.34516	7105	19929	1664,8	1630,2	34.5
$YH_{1.85}$	1.33919	1.27215	6704	18277	1816,7	1782,3	34.4
BeO	1.19678	1.05838	13840	36134	918,9	884,6	34.4
Be	1.27617	1.13823	13794	36133	918,9	884,5	34.4
Gr	1.04104	0.91452	12687	36134	918,9	884,6	34.3

Based on the above summary, several additional remarks can be made on the relative behaviour of the five moderators over the full depletion period: first, $ZrH_{1.6}$ and $YH_{1.85}$ exhibit relatively similar burnup values owing to their similar initial uranium content. Then, as far as the other three configuration(BeO, Be and graphite), due to the fact that they contain significantly less uranium mass ($\approx$ 919 g), they reach significantly higher burnups values ($\approx$ 36 MWd/kgU). while still burning approximately the same absolute weight of Uranium as the hydrides: this indicates that the non-hydrides moderators burn fuel significantly more efficiently over the 10 year lifetime, as per equation 18 below.

$$BU = \frac{time[d] * P_{ass}[MW]}{m_{U,BOL}[kg]} \tag{18}$$

Furthermore, the stronger reactivity swings observed for BeO, Be and Graphite ($\Delta k \approx$ 12 700–13 800 pcm, compared to $\approx$ 7 000 pcm for $YH_{1.85}$ and $ZrH_{1.6}$) are consistent with their higher burnup. Having less fissile material available, each fission represents a larger fraction of the total inventory, resulting in a larger reactivity penalty per unit time of these configurations with respect to those with hydride moderators.

7 Conclusions

The work presented in this thesis has investigated in detail the impact of different solid moderator materials on the neutronic performance of the SELENE nuclear reactor, a compact HALEU-fueled, TRISO-based system conceived to deliver about 100 kWe ($\approx$ 500 kWth) to a lunar outpost over a ten-year mission. The stringent requirements in terms of mass and volume, as well as the specific environmental conditions on the Moon, impose the use of a solid moderator. The selection and optimization of the moderator that best meets these requirements are therefore central drivers of the overall design. In this context, the following five solid moderators were examined: beryllium (Be), beryllium oxide (BeO), graphite, zirconium hydride ($ZrH_{1.6}$) and yttrium hydride ($YH_{1.85}$); all analysis has been performed with the Serpent Monte Carlo code, choosing the ENDF/B-VIII.0 distribution processed in ACE format as the evaluated nuclear data library.

The comparison was made in terms of some crucial neutronic aspects, which were explored in detail through the methodology and then finally presented in chapter 6. Summarizing the process, the first set of results regarded the evaluation of the multiplication factor as a function of the volume-defined moderation ratio; this allowed to find, for each moderator, the configuration with the highest k_∞. Then, the neutron flux spectra were evaluated, together with spectral indexes, to examine the impact of each material on the overall neutron balance in the FA; in the following paragraph, a verification of the literature reviewed moderator parameters, MR and SDP, were made through the calculation of space-energy homogenized cross sections for the specific FA of SELENE reactor, confirming that exists no significant difference between calculated and reference values. The other neutronic evaluations regarded, for the hydrides only, a supplementary analysis which investigated the effect of the H/Metal ratio on the multiplication factor; then, again, for all five moderators, the axial linear power was calculated with and without a BeO reflector. In the end, depletion calculations were performed over the expected operative time of SELENE, 10 years, evaluating each moderator effect on the reactivity swing and fuel burnup.

Based on the results obtained, $ZrH_{1.6}$ can be identified as the most promising moderator for the SELENE concept. In fact, $ZrH_{1.6}$ combines the highest k_∞ at the price of an intermediate moderation ratio, the highest slowing-down power, a balanced spectrum at the optimal configuration and a relatively small reactivity swing over ten years. $YH_{1.85}$,

although slightly less efficient in terms of $k_\infty$and MR, offers, nonetheless, comparable performance in every aspect of the analyzed results, representing a valid alternative with above the average neutronic figures of merit, especially for the depletion features. All the non-hydride moderators, while offering the highest MR values, are penalized by the specific compactness constraints of the SELENE reactor: due to their sensibly lower SDP, all three materials exhibit their maximum k_∞ at the maximum moderator volume (without however reaching a moderation optimum), ruling them away from having an optimized configuration with such high density and small volume requirements. In conclusion, the comparative neutronic evaluation carried out in this thesis supports the selection of metal hydrides, particularly $ZrH_{1.6}$, as the most suitable solid moderator for the SELENE surface nuclear reactor, at least under the current set of assumptions. Future work should extend these FA-level findings to full-core models, including reflectors and control systems, while coupling neutronics with detailed thermal–hydraulic and fuel performance analyses that explicitly account for hydrogen migration, phase stability limits and irradiation-induced degradation of hydrides. Only by integrating these additional multiphysics and materials science aspects it will be possible to confirm whether the neutronic advantages identified here can be translated into an industrially feasible, safe and reliable SNR design for lunar applications.

8 Appendixes A - Tables

Materials' atomic compositions utilized in the simulations; to be noted, the nuclear temperature was set for each nuclide at 1200 K.

Table 13: Homogeneous fuel composition

Isotope	**ao [-]**
Homog. fuel	$\rho = 3.256[\frac{g}{cm^3}]$
O-16	$3,41917 \times 10^{-2}$
O-17	$1,30245 \times 10^{-5}$
O-18	$7,02637 \times 10^{-5}$
U-234	$2,56300 \times 10^{-5}$
U-235	$3,41923 \times 10^{-3}$
U-238	$1,36926 \times 10^{-2}$
C-12	$5,84709 \times 10^{-1}$
C-13	$6,32405 \times 10^{-3}$
Si-28	$3,29748 \times 10^{-1}$
Si-29	$1,67514 \times 10^{-2}$
Si-30	$1,10556 \times 10^{-2}$

Table 14: TRISO material composition

Isotope	**ao [-]**
Kernel	$\rho = 10,4153[\frac{g}{cm^3}]$
O-16	$3,41917 \times 10^{-2}$
O-17	$1,30245 \times 10^{-5}$
O-18	$7,02637 \times 10^{-5}$
U-234	$2,56300 \times 10^{-5}$
U-235	$3,41923 \times 10^{-3}$
U-238	$1,36926 \times 10^{-2}$
Buffer	$\rho = 1,1[\frac{g}{cm^3}]$
C-12	$6,08751 \times 10^{-2}$
C-13	$6,58408 \times 10^{-4}$
iPyC	$\rho = 1,9008[\frac{g}{cm^3}]$
C-12	$6,91596 \times 10^{-2}$
C-13	$7,48012 \times 10^{-4}$
SiC	$\rho = 3,2[\frac{g}{cm^3}]$
Si-28	$3,46701 \times 10^{-2}$
Si-29	$1,76127 \times 10^{-3}$
Si-30	$1,16240 \times 10^{-3}$
C-12	$3,71915 \times 10^{-2}$
C-13	$4,02253 \times 10^{-4}$
oPyC	$\rho = 1,9008[\frac{g}{cm^3}]$
C-12	$1,00945 \times 10^{-1}$
C-13	$1,09180 \times 10^{-3}$
Matrix	$\rho = 3,2[\frac{g}{cm^3}]$
Si-28	$2,95078 \times 10^{-1}$
Si-29	$1,49902 \times 10^{-2}$
Si-30	$9,89319 \times 10^{-3}$
C-12	$3,16537 \times 10^{-1}$
C-13	$3,42358 \times 10^{-3}$

Table 15: Casing material composition

Casing	$\rho = 8.55[\frac{g}{cm^3}]$
Isotope	**ao [-]**
Fe-54	$5,97708 \times 10^{-4}$
Fe-56	$9,38274 \times 10^{-3}$
Fe-57	$2,16688 \times 10^{-4}$
Fe-58	$2,88372 \times 10^{-5}$
Ni-58	$5,13669 \times 10^{-1}$
Ni-60	$1,97863 \times 10^{-1}$
Ni-61	$8,60101 \times 10^{-3}$
Ni-62	$2,74245 \times 10^{-2}$
Ni-64	$6,98328 \times 10^{-3}$
Cr-50	$9,54418 \times 10^{-3}$
Cr-52	$1,84050 \times 10^{-1}$
Cr-53	$2,08698 \times 10^{-2}$
Cr-54	$5,19493 \times 10^{-3}$
Ti-46	$4,92130 \times 10^{-4}$
Ti-47	$4,43812 \times 10^{-4}$
Ti-48	$4,39756 \times 10^{-3}$
Ti-49	$3,22718 \times 10^{-4}$
Ti-50	$3,08998 \times 10^{-4}$
Al-27	$5,71422 \times 10^{-3}$
C-12	$2,35190 \times 10^{-3}$
C-13	$2,54375 \times 10^{-5}$
Y-89	$6,06957 \times 10^{-4}$
O-16	$9,08224 \times 10^{-4}$
O-17	$3,45966 \times 10^{-7}$
O-18	$1,86639 \times 10^{-6}$

Table 16: Wick material composition

Wick	$\rho = 3.12[\frac{g}{cm^3}]$
Isotope	**ao [-]**
Ni-58	$5,06790 \times 10^{-2}$
Ni-60	$1,95214 \times 10^{-2}$
Ni-61	$8,48583 \times 10^{-4}$
Ni-62	$2,70573 \times 10^{-3}$
Ni-64	$6,88976 \times 10^{-4}$
Cr-50	$5,55617 \times 10^{-3}$
Cr-52	$1,07145 \times 10^{-1}$
Cr-53	$1,21494 \times 10^{-2}$
Cr-54	$3,02425 \times 10^{-3}$
Fe-54	$2,60690 \times 10^{-2}$
Fe-56	$4,09227 \times 10^{-1}$
Fe-57	$9,45084 \times 10^{-3}$
Fe-58	$1,25773 \times 10^{-3}$
Mo-92	$1,29443 \times 10^{-3}$
Mo-94	$8,15142 \times 10^{-4}$
Mo-95	$1,41113 \times 10^{-3}$
Mo-96	$1,48507 \times 10^{-3}$
Mo-97	$8,55231 \times 10^{-4}$
Mo-98	$2,17282 \times 10^{-3}$
Mo-100	$8,74830 \times 10^{-4}$
Mn-55	$1,38317 \times 10^{-2}$
Si-28	$1,24760 \times 10^{-2}$
Si-29	$6,33791 \times 10^{-4}$
Si-30	$4,18289 \times 10^{-4}$
C-12	$9,38855 \times 10^{-4}$
C-13	$1,01544 \times 10^{-5}$
P-31	$4,90665 \times 10^{-4}$
S-32	$1,68834 \times 10^{-4}$
S-33	$1,33304 \times 10^{-6}$
S-34	$7,55389 \times 10^{-6}$
S-36	$1,77739 \times 10^{-8}$
N-14	$2,97298 \times 10^{-3}$
N-15	$1,08612 \times 10^{-5}$
Na-23	$3,10807 \times 10^{-1}$

Table 17: Sodium material composition

Sodium	$\rho = 0,0001697[\frac{g}{cm^3}]$
Isotope	**ao [-]**
Na-23	1

Table 18: Be material composition

Be	$\rho = 1,848[\frac{g}{cm^3}]$
Isotope	**ao [-]**
Be-9	1

Table 19: BeO material composition

BeO	$\rho = 3.01[\frac{g}{cm^3}]$
Isotope	**ao [-]**
Be-9	$5,00000 \times 10^{-1}$
O-16	$4,98785 \times 10^{-1}$
O-17	$1,90000 \times 10^{-4}$
O-18	$1,02500 \times 10^{-3}$

Table 20: Graphite material composition

Graphite	$\rho = 1,8[\frac{g}{cm^3}]$
Isotope	**ao [-]**
C-12	1

Table 21: $ZrH_{1.6}$ material composition

$\mathbf{ZrH_{1.6}}$	$\rho = 5.61[\frac{g}{cm^3}]$
Isotope	**ao [-]**
Zr-90	$1,97885 \times 10^{-1}$
Zr-91	$4,31539 \times 10^{-2}$
Zr-92	$6,59615 \times 10^{-2}$
Zr-94	$6,68461 \times 10^{-2}$
Zr-96	$1,07692 \times 10^{-2}$
H-1	$6,15385 \times 10^{-1}$

Table 22: $YH_{1.85}$ material composition

$\mathbf{YH_{1.85}}$	$\rho = 4.24[\frac{g}{cm^3}]$
Isotope	**ao [-]**
H-1	$6,44900 \times 10^{-1}$
H-2	$7,50000 \times 10^{-5}$
Y-89	$3,50900 \times 10^{-1}$

Table 23: Burnup time steps

# step	**TIME [d]**	**TIME [y]**
1	1.87	0.01
2	3.75	0.01
3	7.50	0.02
4	15.00	0.04
5	22.49	0.06
6	29.99	0.08
7	64.98	0.18
8	99.98	0.27
9	149.96	0.41
10	199.95	0.55
11	299.93	0.82
12	399.90	1.09
13	499.88	1.37
14	599.85	1.64
15	699.83	1.92
16	799.80	2.19
17	999.75	2.74
18	1199.70	3.28
19	1399.66	3.83
20	1599.61	4.38
21	1999.51	5.47
22	2399.41	6.57
23	2799.31	7.66
24	3199.21	8.76
25	3599.11	9.85
26	3652.50	10.00

Table 24: SHEM 281-group energy grid

energy bins [MeV]						
2.50E-09	4.56E-09	7.15E-09	1.05E-08	1.48E-08	2.00E-08	2.49E-08
2.93E-08	3.44E-08	4.03E-08	4.73E-08	5.55E-08	6.52E-08	7.65E-08
8.98E-08	1.04E-07	1.20E-07	1.38E-07	1.62E-07	1.90E-07	2.10E-07
2.31E-07	2.55E-07	2.80E-07	3.05E-07	3.25E-07	3.53E-07	3.90E-07
4.32E-07	4.75E-07	5.20E-07	5.55E-07	5.95E-07	6.25E-07	7.20E-07
8.20E-07	8.80E-07	9.20E-07	9.44E-07	9.64E-07	9.82E-07	9.97E-07
1.01E-06	1.02E-06	1.03E-06	1.08E-06	1.09E-06	1.10E-06	1.12E-06
1.13E-06	1.15E-06	1.17E-06	1.21E-06	1.25E-06	1.29E-06	1.33E-06
1.38E-06	1.41E-06	1.44E-06	1.52E-06	1.59E-06	1.67E-06	1.78E-06
1.90E-06	1.99E-06	2.07E-06	2.16E-06	2.22E-06	2.27E-06	2.33E-06
2.47E-06	2.55E-06	2.59E-06	2.62E-06	2.64E-06	2.70E-06	2.72E-06
2.74E-06	2.78E-06	2.88E-06	3.14E-06	3.54E-06	3.71E-06	3.88E-06
4.00E-06	4.22E-06	4.31E-06	4.42E-06	4.77E-06	4.93E-06	5.11E-06
5.21E-06	5.32E-06	5.38E-06	5.41E-06	5.49E-06	5.53E-06	5.62E-06
5.72E-06	5.80E-06	5.96E-06	6.06E-06	6.16E-06	6.28E-06	6.36E-06
6.43E-06	6.48E-06	6.51E-06	6.54E-06	6.56E-06	6.57E-06	6.59E-06
6.61E-06	6.63E-06	6.72E-06	6.74E-06	6.76E-06	6.78E-06	6.79E-06
6.81E-06	6.84E-06	6.87E-06	6.92E-06	6.99E-06	7.14E-06	7.38E-06
7.60E-06	7.74E-06	7.84E-06	7.97E-06	8.13E-06	8.30E-06	8.52E-06
8.67E-06	8.80E-06	8.98E-06	9.14E-06	9.50E-06	1.06E-05	1.08E-05
1.11E-05	1.13E-05	1.16E-05	1.17E-05	1.18E-05	1.20E-05	1.21E-05
1.23E-05	1.25E-05	1.26E-05	1.33E-05	1.35E-05	1.40E-05	1.43E-05
1.45E-05	1.46E-05	1.47E-05	1.49E-05	1.58E-05	1.60E-05	1.66E-05
1.68E-05	1.74E-05	1.76E-05	1.78E-05	1.80E-05	1.91E-05	1.92E-05
1.94E-05	1.96E-05	2.01E-05	2.03E-05	2.04E-05	2.05E-05	2.06E-05
2.07E-05	2.08E-05	2.09E-05	2.10E-05	2.11E-05	2.12E-05	2.13E-05
2.15E-05	2.17E-05	2.20E-05	2.22E-05	2.24E-05	2.25E-05	2.46E-05
2.76E-05	3.37E-05	4.02E-05	4.40E-05	4.58E-05	5.27E-05	6.14E-05
7.50E-05	8.90E-05	1.09E-04	1.33E-04	1.62E-04	1.98E-04	2.42E-04
2.84E-04	3.20E-04	3.54E-04	4.11E-04	5.02E-04	6.13E-04	7.49E-04
9.08E-04	1.06E-03	1.14E-03	1.35E-03	1.61E-03	1.91E-03	2.22E-03
2.58E-03	3.00E-03	3.48E-03	4.10E-03	5.00E-03	6.11E-03	7.47E-03

Continuing in next page...

energy bins [MeV] (continuing)						
9.12E-03	1.11E-02	1.36E-02	1.49E-02	1.62E-02	1.86E-02	2.27E-02
2.50E-02	2.61E-02	2.74E-02	2.93E-02	3.35E-02	3.70E-02	4.09E-02
4.99E-02	5.52E-02	6.74E-02	8.23E-02	9.47E-02	1.16E-01	1.23E-01
1.40E-01	1.65E-01	1.95E-01	2.30E-01	2.68E-01	3.21E-01	3.84E-01
4.13E-01	4.56E-01	4.94E-01	5.78E-01	7.07E-01	8.60E-01	9.51E-01
1.05E+00	1.16E+00	1.29E+00	1.34E+00	1.41E+00	1.64E+00	1.90E+00
2.23E+00	2.73E+00	3.33E+00	4.07E+00	4.97E+00	6.07E+00	6.70E+00
7.41E+00	8.19E+00	9.05E+00	1.00E+01	1.16E+01	1.38E+01	1.49E+01
1.96E+01						

9 Appendixes B - Figures

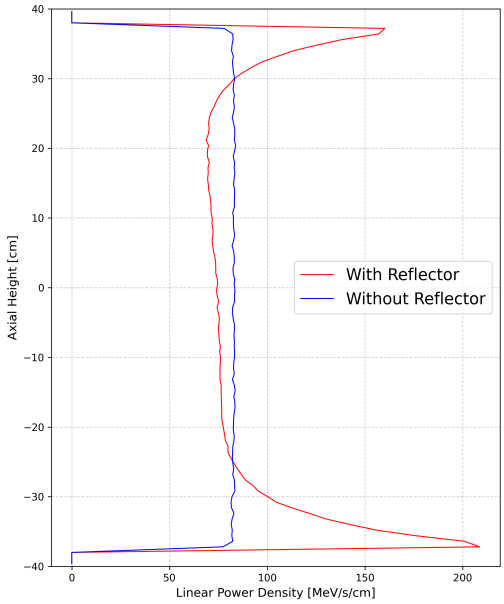

(a) Be

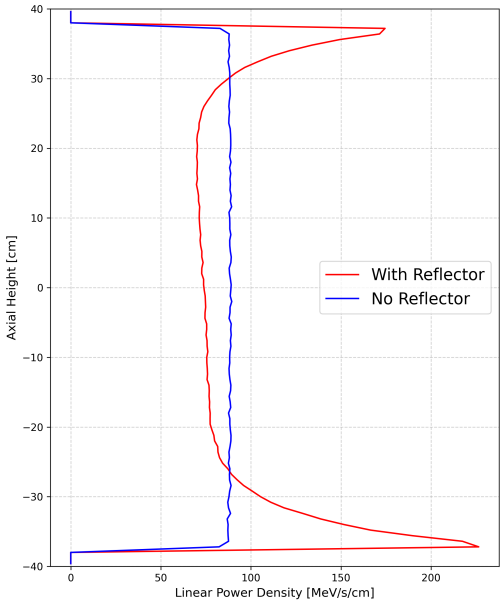

(b) BeO

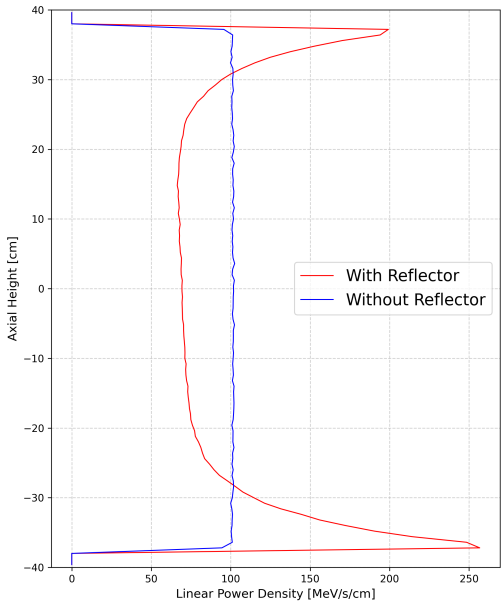

(c) Graphite

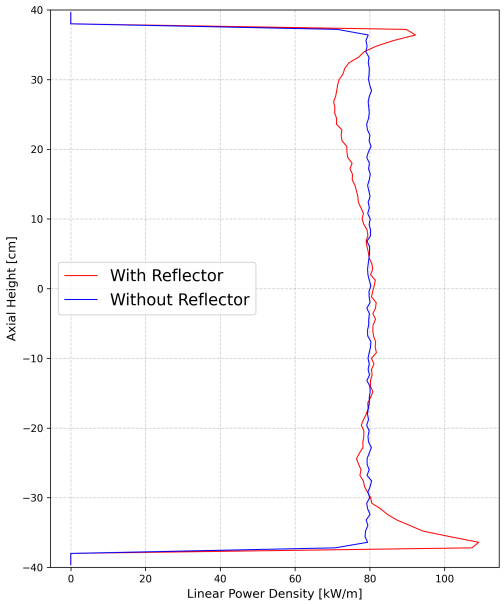

(d) $YH_{1.85}$

Figure 15: Axial linear power direct comparisons **(1/2)**

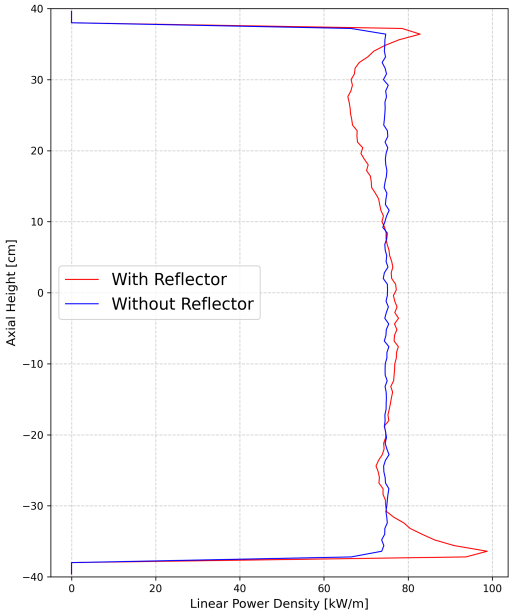

(e) $ZrH_{1.6}$

Figure 15: Axial linear power direct comparisons **(2/2)**

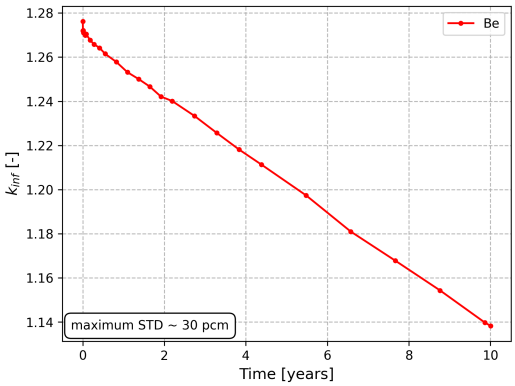

(a) Be

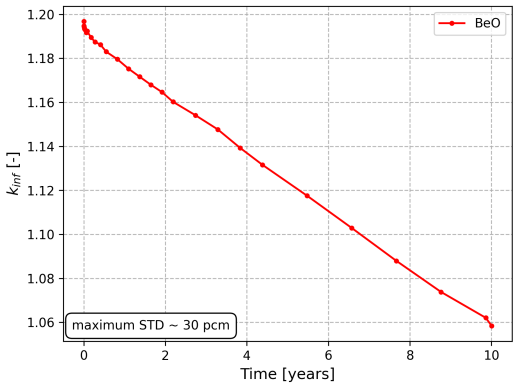

(b) BeO

Figure 16: k_∞ as a function of time **(1/2)**

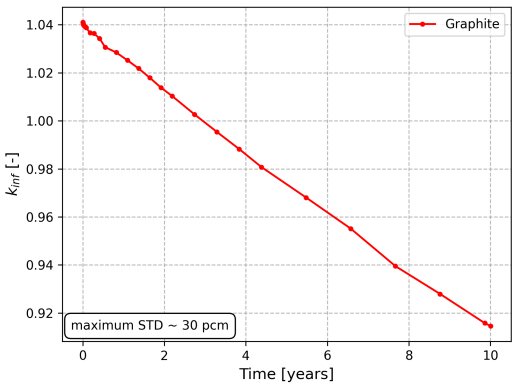

(c) Graphite

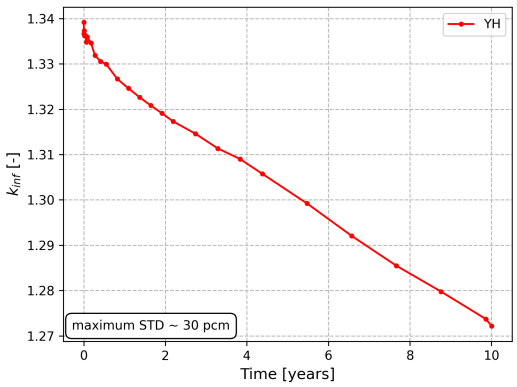

(d) $YH_{1.85}$

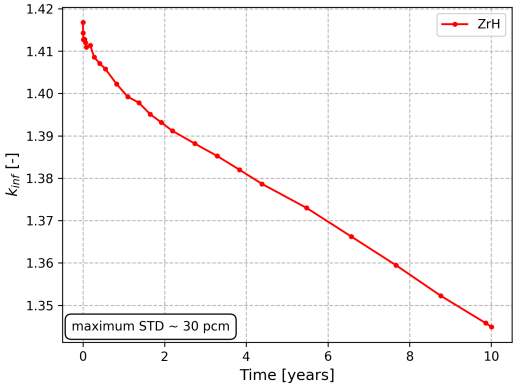

(e) $ZrH_{1.6}$

Figure 16: k_∞ as a function of time **(2/2)**

References

[1] B. J. Ade et al. “Reactor physics considerations for use of yttrium hydride moderator”. In: *Nuclear Science and Engineering* 196.12 (2022), pp. 1539–1558.

[2] D. A. Brown et al. “ENDF/B-VIII. 0: the 8th major release of the nuclear reaction data library with CIELO-project cross sections, new standards and thermal scattering data”. In: *Nuclear data sheets* 148 (2018), pp. 1–142.

[3] C. Carrelli et al. “Towards a feasibility study for a lunar space nuclear reactor, International Astronautical Congress (IAC)”. In: (2024).

[4] X. Chai et al. “Preliminary conceptual design of a moderated micro nuclear reactor core cooled by heat pipe”. In: *Annals of Nuclear Energy* 179 (2022), p. 109399.

[5] M. N. Cinbiz et al. “Considerations for hydride moderator readiness in microreactors”. In: *Nuclear Technology* 209.sup1 (2023), S136–S145.

[6] A. E. Craft and J. C. King. “Reactivity control schemes for fast spectrum space nuclear reactors”. In: *Nuclear Engineering and Design* 241.5 (2011), pp. 1516–1528.

[7] R. S. Detwiler et al. *Compendium of material composition data for radiation transport modeling*. Tech. rep. Pacific Northwest National Laboratory (PNNL), Richland, WA (United States), 2021.

[8] K. Feng et al. “Preliminary analysis of a zirconium hydride moderated megawatt heat pipe reactor”. In: *Nuclear Engineering and Design* 388 (2022), p. 111622.

[9] K. Fu et al. “Experimental investigation and thermodynamic assessment of the yttrium-hydrogen binary system”. In: *Progress in Natural Science: Materials International* 28.3 (2018), pp. 332–336.

[10] X. Hu et al. “Fabrication of yttrium hydride for high-temperature moderator application”. In: *Journal of Nuclear Materials* 539 (2020), p. 152335.

[11] X. Hu et al. *Handbook on the material properties of yttrium hydride for high temperature moderator applications*. Tech. rep. Oak Ridge National Laboratory (ORNL), Oak Ridge, TN (United States), 2021.

[12] K. Kane et al. “Air oxidation of yttrium hydride as a high temperature moderator for thermal neutron spectrum fission reactors”. In: *Journal of Nuclear Materials* 556 (2021), p. 153166.

[13] J. Leppänen et al. “Status of serpent monte carlo code in 2024”. In: *EPJ Nuclear Sciences & Technologies* 11 (2025), p. 3.

[14] C. S. Lin and W. S. Yang. “An assessment of the applicability of multigroup cross sections generated with Monte Carlo method for fast reactor analysis”. In: *Nuclear Engineering and Technology* 52.12 (2020), pp. 2733–2742.

[15] K. B. Palomares. “Moderator Considerations for Space Nuclear Power and Propulsion Systems”. In: *Nuclear and Emerging Technologies for Space 2021*. 2021.

[16] A. Peakman and B. Lindley. “A review of nuclear electric fission space reactor technologies for achieving high-power output and operating with HALEU fuel”. In: *Progress in Nuclear Energy* 163 (2023), p. 104815.

[17] D. I. Poston et al. “KRUSTY reactor design”. In: *Nuclear Technology* 206.sup1 (2020), S13–S30.

[18] J. J. Powers and B. D. Wirth. “A review of TRISO fuel performance models”. In: *Journal of Nuclear Materials* 405.1 (2010), pp. 74–82.

[19] P. Reuss. “Neutron physics”. In: (2008).

[20] V. Rintala et al. “Modeling of realistic pebble bed reactor geometries using the Serpent Monte Carlo code”. In: *Annals of nuclear energy* 77 (2015), pp. 223–230.

[21] R. Sanchez et al. “Kilowatt reactor using stirling TechnologY (KRUSTY) component-critical experiments”. In: *Nuclear Technology* 206.sup1 (2020), S56–S67.

[22] A. Santamarina et al. “Advanced neutronics tools for BWR design calculations”. In: *International Conference on Nuclear Engineering*. Vol. 42452. 2006, pp. 245–254.

[23] A. Stanculescu. *The role of nuclear power and nuclear propulsion in the peaceful exploration of space*. Vol. 1197. IAEA, 2005.

[24] H. Sun et al. “Conceptual design and analysis of a multipurpose micro nuclear reactor power source”. In: *Annals of Nuclear Energy* 121 (2018), pp. 118–127.

[25] H. Trellue et al. “Advancements in yttrium hydride moderator development”. In: *Nuclear Technology* 209.sup1 (2023), S123–S135.

[26] Z. Wang et al. “Advance in and prospect of moderator materials for space nuclear reactors”. In: *International Journal of Energy Research* 45.8 (2021), pp. 11493–11509.

[27] B. Zohuri. *Heat pipe applications in fission driven nuclear power plants*. Springer, 2019.

[28] X. Zou et al. “Analysis of the atomic ratio of H and Zr effect on the neutronics parameters of ZrH moderated space nuclear reactor”. In: *Nuclear Engineering and Technology* 56.12 (2024), pp. 5014–5021.